Linearized Dynamics of General Flux-Pinned Interfaces

Frances Zhu and Mason A. Peck

***Abstract*—A flux-pinned interface offers a passively stable equilibrium that otherwise cannot occur between magnets because electromagnetic fields are divergenceless. The contactless, compliant nature of flux pinning offers many benefits for close-proximity robotic maneuvers, such as rendezvous, docking, and actuation. This paper derives the six degree-of-freedom linear dynamics about an equilibrium for any magnet/superconductor configuration. Linearized dynamics are well suited to predicting close-proximity maneuvers, provide insights into the character of the dynamic system, and are essential for linear control synthesis. The equilibria and stability of a flux-pinned interface are found using Villani's equations for magnetic dipoles. Kordyuk's frozen-image model provides the nonlinear flux-pinning response to these magnetic forces and torques, all of which are then linearized. Comparing simulation results of the nonlinear and linear dynamics shows the extent of the linear model's applicability. Nevertheless, these simple models offer computational speed and physical intuition that a nonlinear model does not.**

***Index Terms*—Dynamics, linear systems, magnetoelectric effects, superconducting magnets.**

I. Introduction

EARNSHAW'S theorem states that there is no stable stationary equilibrium for point charges that are solely held together by electrostatic forces [1]. Because they are also divergenceless, magnetic fields offer no stable equilibria except at the origin or at infinity. This is not the case for flux-pinned magnets, for which a stable equilibrium can exist for any number of magnets at arbitrary relative positions and orientations. Flux pinning a magnet to a superconductor creates an equilibrium, or minimum potential energy well, that stabilizes the magnet's position and orientation.

An external magnetic field excites current vortices within a superconductor, which is a material that carries current without resistance. Cooling a Type II superconductor to below its transition temperature in the presence of a magnetic field establishes permanent current vortices, which persist as long as the superconductor's temperature stays below this threshold. The flux-pinning effect influences the dynamics of kilogram-scale bodies out to about 10 cm of separation distance. The energy in the magnetic field determines the range.

In early empirical studies of flux pinning, Williams noticed potential curves that resemble a volcano, with a minimum at the center of the disc and a maximum near the edge [2]. He proposed a model consisting of a repulsive magnetic field source (the mobile image) superimposed upon an attractive magnetic field source (the frozen image).

There are two conventional methods to model the magnetization of the superconductor: Bean's critical-state model and Kordyuk's frozen-image model [3], [4]. The critical-state model is general but numerically intensive because it is based on a finite-element analysis of interactions among—ideally—infinitesimally small magnetization loops. The accuracy of Bean's model depends on the resolution of magnetization loops, which cannot be feasibly solved in real time for problems of practical interest. Kordyuk's advanced frozen-image model represents the position and orientation of the two images within the superconductor geometrically, an approach that yields drastically simpler and faster real-time representations for feedback-control architectures. The frozen-image model omits the effects from physical parameters such as temperature, material, and geometry, but these may be accounted for in a modified frozen-image model [5]. For simplicity, the following assumptions are made. Critical current density is assumed to be infinite. For familiar problems, this limitation has no practical effect. The induced magnetic field is greater than the first critical magnetic field—again, an issue that rarely arises in practical applications. The temperature is low enough that scaling and hysteretic effects are negligible, although Yang offered a method to incorporate elastic hysteresis [6]. These assumptions, as well as the previous ones, are readily accommodated in systems designed for analyzability. Kordyuk's model and the magnetic moment dipole model provide the foundation for many subsequent analytical assessments of flux-pinned dynamics and are the basis for the rest of this paper [7], [8].

Kordyuk created an analytical model to explain the image effects of flux pinning, known as the frozen-image model [4]. Kordyuk's geometric relation between magnet parameters and image parameters is graphically depicted in–Fig. 2 and further discussed in Section II. Other authors (Alqadi [9], Cansiz [10], Suguira [11], etc.) have written primarily about finding the potential fields of magnet/superconductor arrangements or the equilibria of magnet/superconductor arrangements in three or less degrees of freedom. This paper derives the most general case of six degrees of freedom.

Manuscript received August 8, 2017; revised April 5, 2018; accepted May 30, 2018. This work was supported in part by the NASA Space Technology Research Fellowship under Grant NNX15AP55H. This paper was recommended by Associate Editor Philippe J. Masson. *(Corresponding author: Frances Zhu.)*

The authors are with the Department of Mechanical and Aerospace Engineering, Cornell University, Ithaca, NY 14853 USA (e-mail: fz55@cornell.edu; mp336@cornell.edu).

Color versions of one or more of the figures in this paper are available online at http://ieeexplore.ieee.org.

Digital Object Identifier 10.1109/TASC.2018.2844375

Q1 Fig. 1. Cryocooled superconductor with a pinned permanent magnet suspended in gravity.

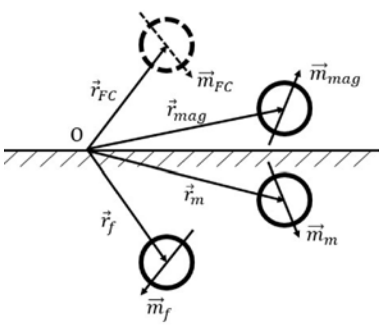

Fig. 2. Geometric relationship among the equilibrium, frozen image, mobile image, superconductor and magnet [4].

A flux-pinned interface offers many benefits for robotics applications, namely, passive stability, compliance, absence of mechanical contact, and low mass requirements. Flux-pinned systems can be actively manipulated to control the orientation and position of close-proximity vehicles while remaining contactless and compliant [12]. Traditional, linear control synthesis may be successful for such systems, but the inherently nonlinear dynamics must be linearized to provide a suitable plant model. A linearized model also provides valuable insights into the system, such as stability, natural frequencies, and modes. This study focuses on a general, linear model for these reasons.

II. Magnetic Field Sources

The general expression for magnetic field strength at distance $\boldsymbol{\rho}$ from the field source is (1) [10]. $\boldsymbol{m}$ is the magnetic moment of the dipole of interest. From (1), the magnetic field strength decreases with distance cubed. The expression for magnetic field strength can be related to a flux-pinned mobile image, flux-pinned frozen image, electromagnet, or permanent magnet. The magnetic field is a function of two variables: $\boldsymbol{m}$ the magnetic moment dipole and $\boldsymbol{\rho}$ the distance from the field source. $\boldsymbol{m}$ is a parameter determined by the physical nature of the source. $\boldsymbol{\rho}$ can be defined or measured in the physical system. The expression for magnetic moment dipoles differs for each type magnetic field source.

$$\boldsymbol{B}(\boldsymbol{\rho}) = \frac{\mu_0}{4\pi|\boldsymbol{\rho}|^3}\left(3\left(\boldsymbol{m}\cdot\hat{\boldsymbol{\rho}}\right)\hat{\boldsymbol{\rho}} - \hat{\boldsymbol{m}}\right). \tag{1}$$

A. Physical Magnet

There are two types of physical magnetic field sources: permanent magnets and electromagnets. The magnetic moment dipole of a permanent magnet is purely defined by physical characteristics in (2). B_0 is the manufacturer's measurement of the magnetic field at the surface of the magnet. d is the distance from the center of dipole to the surface. $\hat{\boldsymbol{m}}_{\boldsymbol{p}}$ is the unit direction of the magnetic moment dipole. The electromagnetic moment dipole is represented by (3), where $V(t)$ is the voltage potential of the electromagnet, A is the area enclosed by the electromagnet's coil of wire, T is the number of turns of the electromagnet, and R is the resistance of the electromagnet. Besides their physical differences, they mathematically represent a physical magnetic moment dipole $\boldsymbol{m}_{\boldsymbol{p}}$. Fig. 3(a) graphically depicts the relationship among variables. The two physical magnetic field sources differ in the physical parameters that make up the magnetic moment dipole expression.

$$\boldsymbol{m}_{\boldsymbol{p}} = \frac{2\pi B_0 d^3}{\mu_0}\hat{\boldsymbol{m}}_{\boldsymbol{p}} \tag{2}$$

$$\boldsymbol{m}_{\boldsymbol{E}} = \frac{VAT}{R}\hat{\boldsymbol{m}}_{\boldsymbol{E}}. \tag{3}$$

B. Mobile/Diamagnetic Image

All superconductors display the Meissner effect, which is the expulsion of magnetic flux. The magnetic source that creates the Meissner effect may be represented as an image within the superconductor that changes the polarity and magnitude to always repel. That image, more specifically, follows the external magnetic source and reorients to the moment dipole to mirror the external magnetic source. The mobile image's magnetic moment dipole depends on the permanent magnet's moment dipole and the orientation of the superconductor, given by (4). $\boldsymbol{m}_{\boldsymbol{mag}}$ is the vector from (2) or (3) that represents the physical magnet's moment dipole. $\hat{\boldsymbol{m}}_{\boldsymbol{s}}$ is the unit direction normal to the surface of the superconductor, illustrated in Fig. 3(b). The mobile image moves when the permanent magnet moves, so the location of the magnetic field from the mobile image is dynamic. $\boldsymbol{r}_{\boldsymbol{mag}}$ and $\boldsymbol{r}_{\boldsymbol{m}}$ change in the expression for magnetic field and potential energy, respectively. The magnetic field of the magnet's mobile image from Fig. 3(b) is given by (5), where $\boldsymbol{\rho}_{\boldsymbol{m}}$ is the distance from the mobile image to the permanent magnet that is given by (6), where $\boldsymbol{r}_{\boldsymbol{m}}$ is the location of the mobile image and $\boldsymbol{O}_{\boldsymbol{s}}$ is a point on the superconductor surface. The mobile image's magnetic moment dipole location and orientation are dependent on the superconductor's geometry.

$$\boldsymbol{m}_{\boldsymbol{m}} = \boldsymbol{m}_{\boldsymbol{mag}} - 2\left(\hat{\boldsymbol{m}}_{\boldsymbol{s}}\cdot\boldsymbol{m}_{\boldsymbol{mag}}\right)\hat{\boldsymbol{m}}_{\boldsymbol{s}} \tag{4}$$

$$\boldsymbol{\rho}_{\boldsymbol{m}} = \boldsymbol{r}_{\boldsymbol{mag}} - \boldsymbol{r}_{\boldsymbol{m}} \tag{5}$$

$$\boldsymbol{r}_{\boldsymbol{m}} = \boldsymbol{r}_{\boldsymbol{mag}} - 2\left(\left(\boldsymbol{r}_{\boldsymbol{mag}} - \boldsymbol{O}_{\boldsymbol{s}}\right)\cdot\hat{\boldsymbol{m}}_{\boldsymbol{s}}\right)\hat{\boldsymbol{m}}_{\boldsymbol{s}}. \tag{6}$$

C. Physical Magnet

The frozen image is an image specific to high temperature or Type II superconductors. Instead of expelling all magnetic

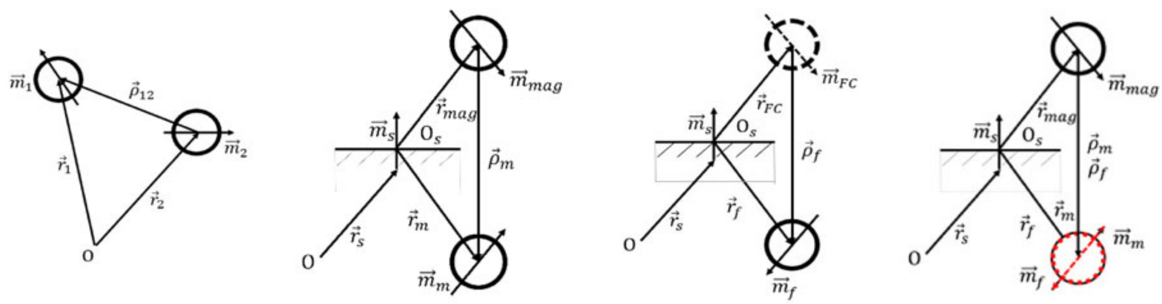

Fig. 3. Different types of magnetic field interactions. (a) Geometric representation of permanent magnet or electromagnet magnetic field source positions. (b) Geometric representation of mobile image magnetic field source positions. (c) Geometric representation of frozen-image magnetic field source positions. (d) Geometric representation of frozen image and mobile image overlaid at field-cooled position.

flux like Type I superconductors do, Type II superconductors field-cool a magnetic field during a transition phase and expel external fields that differ from the embedded field. This property allows for the stable presence of a field, in this application, infinitesimal magnetic dipole. The frozen image is a consequence of the presence of an infinitesimal magnetic dipole *a priori* and *a posteriori* cryocooling, which embeds a field in the superconductor that enforces restoration to this initial state. To counter the mobile image's repulsion, the frozen image acts as an attractive infinitesimal magnetic dipole that stays in place and aligns magnetic moment dipoles with the field-cooled magnet. The frozen image's magnetic moment dipole depends on the magnetic moment dipole field-cooled onto the superconductor and the orientation of the superconductor, as shown in (7) and geometrically in Fig. 3(c). Equations (8) and (9) are analogous to the frozen-image distance vectors. Like the mobile image, the frozen image is dependent on the superconductor's geometry, but, unlike the mobile image, it does not move when the permanent magnet moves after field cooling.

$$\boldsymbol{m_f} = 2\,(\hat{\boldsymbol{m}}_s \cdot \boldsymbol{m_{FC}})\,\hat{\boldsymbol{m}}_s - \boldsymbol{m_{FC}} \tag{7}$$

$$\boldsymbol{\rho_f} = \boldsymbol{r_{FC}} - \boldsymbol{r_f} \tag{8}$$

$$\boldsymbol{r_f} = \boldsymbol{r_{FC}} - 2\,((\boldsymbol{r_{FC}} - \boldsymbol{O}_s)\cdot \hat{\boldsymbol{m}}_s)\,\hat{\boldsymbol{m}}_s. \tag{9}$$

III. Linearized Dynamics for a Single Flux-Pinned Magnet and Superconductor Interaction

The linearized dynamics for the simplest flux-pinned interface is derived. The dynamics are solely dependent on the magnetic field source's position and orientation, along with physical parameters specific to the system geometry. Each subsection describes the linearization process briefly before presenting the final linearized equation set.

A. Linearizing General Magnetic Dipole Force and Torque Equations

Villani derived the force of a magnetic dipole $\boldsymbol{m_b}$ acting on another magnetic dipole $\boldsymbol{m_a}$ at distance $\boldsymbol{\rho}$, given by (10) shown at the bottom of this page, in which the scalars are brought out front and all vectors are unit direction vectors [4]. The final linearized force equation relates the first-order terms $\delta\boldsymbol{F_{ab}}$ to $\delta\boldsymbol{r}$, $\delta\boldsymbol{m_a}$, and $\delta\boldsymbol{m_b}$, all vectors denoting deviation from equilibrium. To linearize about $\boldsymbol{\rho_e}$, $\boldsymbol{m_{ae}}$, and $\boldsymbol{m_{be}}$, a first-order Taylor expansion of (10) was taken by replacing $\boldsymbol{F_{ab}} = \boldsymbol{F_e} + \delta\boldsymbol{F_{ab}}$, $\boldsymbol{\rho} = \boldsymbol{\rho_e} + \delta\boldsymbol{r}$, $\boldsymbol{m_a} = \boldsymbol{m_{ae}} + \delta\boldsymbol{m_a}$, and $\boldsymbol{m_b} = \boldsymbol{m_{be}} + \delta\boldsymbol{m_b}$. The equilibrium force is subtracted from both sides. The cross products and dot products are replaced with cross and transpose operators ($v\times$ to $v^\times$ and $v\cdot$ to v^T), and then rearranged to isolate the first-order terms. To transform the linear equation to matrix form, notice that the quantities in front of $\delta\boldsymbol{r}$, $\delta\boldsymbol{m_a}$, and $\delta\boldsymbol{m_b}$ are 3 $\times$ 3 matrices. The final matrix expression for linearized force between two magnetic moment dipoles is given by (11) shown at the bottom of this page. The moment/torque of a magnetic dipole $\boldsymbol{m_b}$ acting on another magnetic dipole $\boldsymbol{m_a}$ at distance ρ is given by (12), shown at the top of the next page, also derived by Villani [5]. The same process of linearization is applied to Villani's moment equation to yield (13) shown at the top of the next page.

B. Linearized Forces and Torques for Flux-Pinned Forces and Torques

The total force from a flux-pinned interaction is the superposition of the mobile image force and frozen-image force. These

$$\boldsymbol{F_{ab}} = \frac{3\mu_0 m_a m_b}{4\pi\rho^4}\left((\hat{\boldsymbol{\rho}}\times\hat{\boldsymbol{m}}_{\boldsymbol{a}})\times\hat{\boldsymbol{m}}_{\boldsymbol{b}} + (\hat{\boldsymbol{\rho}}\times\hat{\boldsymbol{m}}_{\boldsymbol{b}})\times\hat{\boldsymbol{m}}_{\boldsymbol{a}} - 2\hat{\boldsymbol{\rho}}\,(\hat{\boldsymbol{m}}_{\boldsymbol{a}}\cdot\hat{\boldsymbol{m}}_{\boldsymbol{b}}) + 5\hat{\boldsymbol{\rho}}\,((\hat{\boldsymbol{\rho}}\times\hat{\boldsymbol{m}}_{\boldsymbol{a}})\cdot(\hat{\boldsymbol{\rho}}\times\hat{\boldsymbol{m}}_{\boldsymbol{b}}))\right) \tag{10}$$

$$\delta\boldsymbol{F_{ab}} = \frac{3\mu_0}{4\pi|\rho_e|^5}\begin{bmatrix} m_{be}^\times m_{ae}^\times + m_{ae}^\times m_{be}^\times - 2m_{ae}^T m_{be}\underline{1} - \frac{5}{|\rho_e|^2}\left(\rho_e\left(\rho_e^\times m_{be}\right)^T m_{ae}^\times - \rho_e\left(\rho_e^\times m_{ae}\right)^T m_{be}^\times\right) + \cdots \\ -\frac{5}{|\rho_e|^2}\left(\left(\rho_e^\times m_{ae}\right)^\times m_{be} + \left(\rho_e^\times m_{be}\right)^\times m_{ae} - 2\left(m_{ae}^T m_{be}\right)\rho_e + \frac{5}{|\rho_e|^2}\left(\left(\rho_e^\times m_{ae}\right)^T\left(\rho_e^\times m_{be}\right)\right)\rho_e^T\right) \\ -m_{be}^\times\rho_e^\times + \left(\rho_e^\times m_{be}\right)^\times - 2\rho_e m_{be}^T + \frac{5}{|\rho_e|^2}\rho_e\left(\rho_e^\times m_{be}\right)^T\rho_e^\times \\ \left(\rho_e m_{ae}\right)^\times - m_{ae}^\times\rho_e^\times - 2\rho_e m_{ae}^T + \frac{5}{|\rho_e|^2}\rho_e\left(\rho_e^\times m_{ae}\right)^T\rho_e^\times \end{bmatrix}^T \begin{bmatrix}\delta\boldsymbol{r}\\ \delta\boldsymbol{m_a}\\ \delta\boldsymbol{m_b}\end{bmatrix} \tag{11}$$

$$\boldsymbol{\tau_{ab}} = \frac{\mu_0 m_a m_b}{4\pi \rho^3}\left(3\left(\hat{\boldsymbol{m}}_{\boldsymbol{a}} \cdot \hat{\boldsymbol{\rho}}\right)\left(\hat{\boldsymbol{m}}_{\boldsymbol{b}} \times \hat{\boldsymbol{\rho}}\right) + \left(\hat{\boldsymbol{m}}_{\boldsymbol{a}} \times \hat{\boldsymbol{m}}_{\boldsymbol{b}}\right)\right) \tag{12}$$

$$\delta\boldsymbol{\tau_{ab}} = \frac{\mu_0}{4\pi|\rho_e|^3}\begin{bmatrix} \frac{3}{|\rho_e|^2}\left(m_{ae}^T\rho_e m_{be}^\times + m_{be}^T\rho_e m_{ae}^\times - \left(\frac{3}{|\rho_e|^2}m_{ae}^T\rho_e m_{be}^\times\rho_e + m_{ae}^\times m_{be}\right)\rho_e^T\right) \\ \frac{3}{|\rho_e|^2}m_{be}^\times\rho_e\rho_e^T - m_{be}^\times \\ -\frac{3}{|\rho_e|^2}m_{ae}^\times\rho_e\rho_e^T - m_{ae}^\times \end{bmatrix}\begin{bmatrix}\delta\boldsymbol{r} \\ \delta\boldsymbol{m_a} \\ \delta\boldsymbol{m_b}\end{bmatrix}. \tag{13}$$

images are magnetic field sources that impart linearized forces given by (11). The frozen-image force is found by substituting $\boldsymbol{m_{ae}}$ to $\boldsymbol{m_e}$, the magnet's equilibrium magnetic moment dipole, and $\boldsymbol{m_{be}}$ to $\boldsymbol{m_{fe}}$, the frozen image's equilibrium magnetic moment dipole, into (11). The frozen image will never change in orientation; thus, $\delta\boldsymbol{m_f} = 0$. The linearized force from the frozen image is given by (14) shown at the bottom of this page. The mobile image force, given by (16), is similarly obtained by substituting $\boldsymbol{m_{ae}}$ to $\boldsymbol{m_e}$, the magnet's equilibrium magnetic moment dipole, and $\boldsymbol{m_{be}}$ to $\boldsymbol{m_{me}}$, the mobile image's equilibrium magnetic moment dipole, into (11). From Kordyuk's geometric interpretation of the frozen-image model, the mobile image reorients itself like a mirror image across the superconductors surface, where $\hat{\boldsymbol{m}}_{\boldsymbol{s}}$ is the unit normal to the superconductor's surface given by (4). A direct relation from $\boldsymbol{m}$ to $\boldsymbol{m_m}$ is given by (15) shown at the bottom of this page. This relationship reduces the number of independent state variables. The mobile image force equation depends only on the magnet's orientation and position, given by (16) shown at the bottom of this page. The forces from the mobile and frozen images are additive and may be combined to a final equation for force on the system, given by (17) shown at the bottom of this page. The total force is dependent on the physical magnet's position and orientation, which constitutes the translational dynamic state of the flux-pinned interaction.

The total torque from a flux-pinned interface is the sum of the combined frozen and mobile image effects. The frozen-image torque is obtained by substituting $\boldsymbol{m_{ae}}$ to $\boldsymbol{m_e}$, the magnet's equilibrium magnetic moment dipole, and $\boldsymbol{m_{be}}$ to $\boldsymbol{m_{fe}}$, the frozen image's equilibrium magnetic moment dipole. The orientation of the frozen image does not change, so the state $\delta\boldsymbol{m_f}$ and the corresponding coefficient are excluded, given by (18) shown at the top of the next page. The same process is applied to the mobile image. Substituting (15) into our previous equation, we

$$\delta\boldsymbol{F_f} = \frac{3\mu_0}{4\pi|\rho_e|^5}\begin{bmatrix} m_{fe}^\times m_e^\times + m_e^\times m_{fe}^\times - 2m_e^T m_{fe}\underline{1} - \frac{5}{|\rho_e|^2}\left(\rho_e\left(\rho_e^\times m_{fe}\right)^T m_e^\times - \rho_e\left(\rho_e^\times m_e\right)^T m_{fe}^\times\right) + \cdots \\ -\frac{5}{|\rho_e|^2}\left(\left(\rho_e^\times m_e\right)^\times m_{fe} + \left(\rho_e^\times m_{fe}\right)^\times m_e - 2\left(m_e^T m_{fe}\right)\rho_e + \frac{5}{|\rho_e|^2}\left(\left(\rho_e^\times m_e\right)^T\left(\rho_e^\times m_{fe}\right)\right)\rho_e^T\right) \\ -m_{fe}^\times\rho_e^\times + \left(\rho_e^\times m_{fe}\right)^\times - 2\rho_e m_{fe}^T + \frac{5}{|\rho_e|^2}\rho_e\left(\rho_e^\times m_{fe}\right)^T\rho_e^\times \end{bmatrix}^T\begin{bmatrix}\delta\boldsymbol{r} \\ \delta\boldsymbol{m}\end{bmatrix} \tag{14}$$

$$\boldsymbol{m_m} = \left(\underline{1} - 2\hat{m}_s\hat{m}_s^T\right)\boldsymbol{m} \tag{15}$$

$$\delta\boldsymbol{F_m} = \frac{3\mu_0}{4\pi|\rho_e|^5}\begin{bmatrix} 2\hat{m}_s\hat{m}_s^T\left(m_{me}^\times m_e^\times + m_e^\times m_{me}^\times - 2m_e^T m_{me}\underline{1} - \frac{5}{|\rho_e|^2}\left(\rho_e\left(\rho_e^\times m_{me}\right)^T m_e^\times - \rho_e\left(\rho_e^\times m_e\right)^T m_{me}^\times\right) + \cdots \right. \\ \left. -\frac{5}{|\rho_e|^2}\left(\left(\rho_e^\times m_e\right)^\times m_{me} + \left(\rho_e^\times m_{me}\right)^\times m_e - 2\left(m_e^T m_{me}\right)\rho_e + \frac{5}{|\rho_e|^2}\left(\left(\rho_e^\times m_e\right)^T\left(\rho_e^\times m_{me}\right)\right)\rho_e^T\right)\right) \\ -m_{me}^\times\rho_e^\times + \left(\rho_e^\times m_{me}\right)^\times - 2\rho_e m_{me}^T + \frac{5}{|\rho_e|^2}\rho_e\left(\rho_e^\times m_{me}\right)^T\rho_e^\times + \cdots \\ \left(\underline{1} - 2\hat{m}_s\hat{m}_s^T\right)\left(\left(\rho_e m_e\right)^\times - m_e^\times\rho_e^\times - 2\rho_e m_e^T + \frac{5}{|\rho_e|^2}\rho_e\left(\rho_e^\times m_e\right)^T\rho_e^\times\right) \end{bmatrix}^T\begin{bmatrix}\delta\boldsymbol{r} \\ \delta\boldsymbol{m}\end{bmatrix} \tag{16}$$

$$\delta\boldsymbol{F_{tot}} = \frac{3\mu_0}{4\pi|\rho_e|^5}\begin{bmatrix} m_{fe}^\times m_e^\times + m_e^\times m_{fe}^\times - 2m_e^T m_{fe}\underline{1} - \frac{5}{|\rho_e|^2}\left(\rho_e\left(\rho_e^\times m_{fe}\right)^T m_e^\times - \rho_e\left(\rho_e^\times m_e\right)^T m_{fe}^\times\right) + \cdots \\ -\frac{5}{|\rho_e|^2}\left(\left(\rho_e^\times m_e\right)^\times m_{fe} + \left(\rho_e^\times m_{fe}\right)^\times m_e - 2\left(m_e^T m_{fe}\right)\rho_e + \frac{5}{|\rho_e|^2}\left(\left(\rho_e^\times m_e\right)^T\left(\rho_e^\times m_{fe}\right)\right)\rho_e^T\right) + \cdots \\ 2\hat{m}_s\hat{m}_s^T\left(m_{me}^\times m_e^\times + m_e^\times m_{me}^\times - 2m_e^T m_{me}\underline{1} - \frac{5}{|\rho_e|^2}\left(\rho_e\left(\rho_e^\times m_{me}\right)^T m_e^\times - \rho_e\left(\rho_e^\times m_e\right)^T m_{me}^\times\right) + \cdots \right. \\ \left. -\frac{5}{|\rho_e|^2}\left(\left(\rho_e^\times m_e\right)^\times m_{me} + \left(\rho_e^\times m_{me}\right)^\times m_e - 2\left(m_e^T m_{me}\right)\rho_e + \frac{5}{|\rho_e|^2}\left(\left(\rho_e^\times m_e\right)^T\left(\rho_e^\times m_{me}\right)\right)\rho_e^T\right)\right) \\ -m_{fe}^\times\rho_e^\times + \left(\rho_e^\times m_{fe}\right)^\times - 2\rho_e m_{fe}^T + \frac{5}{|\rho_e|^2}\rho_e\left(\rho_e^\times m_{fe}\right)^T\rho_e^\times + \cdots \\ -m_{me}^\times\rho_e^\times + \left(\rho_e^\times m_{me}\right)^\times - 2\rho_e m_{me}^T + \frac{5}{|\rho_e|^2}\rho_e\left(\rho_e^\times m_{me}\right)^T\rho_e^\times + \cdots \\ \left(\underline{1} - 2\hat{m}_s\hat{m}_s^T\right)\left(\left(\rho_e m_e\right)^\times - m_e^\times\rho_e^\times - 2\rho_e m_e^T + \frac{5}{|\rho_e|^2}\rho_e\left(\rho_e^\times m_e\right)^T\rho_e^\times\right) \end{bmatrix}^T\begin{bmatrix}\delta\boldsymbol{r} \\ \delta\boldsymbol{m}\end{bmatrix}. \tag{17}$$

$$\delta\boldsymbol{\tau}_{\boldsymbol{f}} = \frac{\mu_0}{4\pi|\rho_e|^3}\begin{bmatrix} \frac{3}{|\rho_e|^2}\left(m_e^T\rho_e m_{fe}^{\times} + m_{fe}^T\rho_e m_e^{\times} - \left(\frac{3}{|\rho_e|^2}m_e^T\rho_e m_{fe}^{\times}\rho_e + m_e^{\times}m_{fe}\right)\rho_e^T\right) \\ \frac{3}{|\rho_e|^2}m_{fe}^{\times}\rho_e\rho_e^T - m_{fe}^{\times} \end{bmatrix}^T \begin{bmatrix} \delta\boldsymbol{r} \\ \delta\boldsymbol{m} \end{bmatrix} \tag{18}$$

$$\delta\boldsymbol{\tau}_{\boldsymbol{m}} = \frac{\mu_0}{4\pi|\rho_e|^3}\begin{bmatrix} 2\hat{m}_s\hat{m}_s^T\left(\frac{3}{|\rho_e|^2}\left(m_e^T\rho_e m_{me}^{\times} + m_{me}^T\rho_e m_e^{\times} - \left(\frac{3}{|\rho_e|^2}m_e^T\rho_e m_{me}^{\times}\rho_e + m_e^{\times}m_{me}\right)\rho_e^T\right)\right) \\ \frac{3}{|\rho_e|^2}m_{me}^{\times}\rho_e\rho_e^T - m_{me}^{\times} + \left(2\hat{m}_s\hat{m}_s^T - \underline{1}\right)\left(\frac{3}{|\rho_e|^2}m_e^{\times}\rho_e\rho_e^T + m_e^{\times}\right) \end{bmatrix}^T \begin{bmatrix} \delta r \\ \delta m \end{bmatrix} \tag{19}$$

$$\delta\boldsymbol{\tau}_{\boldsymbol{tot}} = \frac{\mu_0}{4\pi|\rho_e|^3}\begin{bmatrix} \frac{3}{|\rho_e|^2}\left(m_e^T\rho_e m_{fe}^{\times} + m_{fe}^T\rho_e m_e^{\times} - \left(\frac{3}{|\rho_e|^2}m_e^T\rho_e m_{fe}^{\times}\rho_e + m_e^{\times}m_{fe}\right)\rho_e^T\right) + \cdots \\ 2\hat{m}_s\hat{m}_s^T\left(\frac{3}{|\rho_e|^2}\left(m_e^T\rho_e m_{me}^{\times} + m_{me}^T\rho_e m_e^{\times} - \left(\frac{3}{|\rho_e|^2}m_e^T\rho_e m_{me}^{\times}\rho_e + m_e^{\times}m_{me}\right)\rho_e^T\right)\right) \\ \frac{3}{|\rho_e|^2}m_{fe}^{\times}\rho_e\rho_e^T - m_{fe}^{\times} + \frac{3}{|\rho_e|^2}m_{me}^{\times}\rho_e\rho_e^T - m_{me}^{\times} + \left(2\hat{m}_s\hat{m}_s^T - \underline{1}\right)\left(\frac{3}{|\rho_e|^2}m_e^{\times}\rho_e\rho_e^T + m_e^{\times}\right) \end{bmatrix}^T \begin{bmatrix} \delta\boldsymbol{r} \\ \delta\boldsymbol{m} \end{bmatrix}. \tag{20}$$

reduce the number of states needed to calculate $\delta\boldsymbol{m}_{\boldsymbol{m}}$ given by (19) shown at the top of the next page. The total torque on the magnet is the sum of the torque from the mobile and frozen images, given by (20) shown at the top of this page. The total torque is solely dependent on the physical magnet's position and orientation, which constitutes the rotational dynamic state of the flux-pinned interaction.

C. Governing Equations

For the case of a single magnet and single superconductor, the magnet's dynamics are due to the forces and torques from the frozen and mobile images. In this single magnet case, there are two magnet moment dipoles that are exerting forces and torques on the magnet. The force and torque equations are given by (21) and (22), respectively. The translational dynamics of the flux-pinned magnet is a result of the force balance equation (23). The linear momentum balance, given by (24), is put into matrix form to be easily inserted into a state-space form later. Euler's rigid body equation (25) propagates attitude dynamics. The linearized version of the rigid body equations is given by (26). Equation (27) simplifies to no longer include the gyroscopic dynamics because the magnitude of angular velocity at equilibrium is 0. The orientation of the magnet may be represented by an Euler axis-angle (28), and alternatively by a quaternion (29). In this case, the Euler axis is the magnetic moment dipole unit vector, and the angle may be chosen to be π because the magnet is axisymmetric. Choosing π retains most of the information about the magnetic moment dipole-pointing vector. Upon inspection, the fourth component of the quaternion about equilibrium will always be zero; thus, no information is lost if the quaternion state vector is shortened to just the vector components q_v. To propagate the attitude dynamics, there is a linear relation between the quaternion and angular velocity that yields the quaternion derivative, given by (30). This set of equations fully defines the linearized dynamics of a rigid body.

$$\sum \boldsymbol{F} = \boldsymbol{F}_f + \boldsymbol{F}_{\boldsymbol{m}} \tag{21}$$

$$\sum \boldsymbol{\tau} = \boldsymbol{\tau}_f + \boldsymbol{\tau}_{\boldsymbol{m}} \tag{22}$$

$$\sum \boldsymbol{F} = M\ddot{\boldsymbol{r}} \tag{23}$$

$$\delta\ddot{\boldsymbol{r}} = \boldsymbol{M}^{-1}\delta\boldsymbol{F}_{\boldsymbol{tot}} \tag{24}$$

$$\boldsymbol{\tau} = I\cdot\dot{\boldsymbol{\omega}} + \boldsymbol{\omega}\times(I\cdot\boldsymbol{\omega}) \tag{25}$$

$$\delta\dot{\omega} = I^{-1}\left(\omega_e^{\times}I - (I\omega_e)^{\times}\right)\delta\omega + I^{-1}\tau \tag{26}$$

$$\delta\dot{\omega} = I^{-1}\delta\tau \tag{27}$$

$$\delta\boldsymbol{m} = \theta\delta\hat{\boldsymbol{m}} \tag{28}$$

$$\delta q = \begin{bmatrix} \delta\hat{\boldsymbol{m}}\sin\left(\frac{\theta}{2}\right) \\ \cos\left(\frac{\theta}{2}\right) \end{bmatrix} \tag{29}$$

$$\delta\dot{\boldsymbol{q}}_{\boldsymbol{v}} = \frac{1}{2}\boldsymbol{q}_{\boldsymbol{ve}}\times\delta\boldsymbol{\omega}. \tag{30}$$

D. State-Space Model

The single magnet flux-pinned system dynamics may be represented with a first-order system state-space matrix, given by (31). The state matrix has the form given in (32). Each entry in the state matrix is a block matrix of size corresponding to the state and resultant, where the following a_{ij} values are given by (34)–(40). The matrix entries a_{ij} are block matrices of size 3×3 that are generated from the linearized forces and torques from (17) and (20), respectively. Eq. (37)."(40) shown at the bottom of the next page.

$$\begin{bmatrix} \delta\dot{\boldsymbol{r}} \\ \delta\ddot{\boldsymbol{r}} \\ \delta\dot{\boldsymbol{q}}_{\boldsymbol{v}} \\ \delta\dot{\boldsymbol{\omega}} \end{bmatrix} = A\begin{bmatrix} \delta\boldsymbol{r} \\ \delta\dot{\boldsymbol{r}} \\ \delta\boldsymbol{q}_{\boldsymbol{v}} \\ \delta\boldsymbol{\omega} \end{bmatrix} \tag{31}$$

$$\begin{bmatrix} \delta\dot{\boldsymbol{r}} \\ \delta\ddot{\boldsymbol{r}} \\ \delta\dot{\boldsymbol{q}}_{\boldsymbol{v}} \\ \delta\dot{\boldsymbol{\omega}} \end{bmatrix} = \begin{bmatrix} 0 & \underline{1} & 0 & 0 \\ a_{21} & 0 & a_{23} & 0 \\ 0 & 0 & 0 & \frac{1}{2}q_{ve}^{\times} \\ a_{41} & 0 & a_{43} & 0 \end{bmatrix}\begin{bmatrix} \delta\boldsymbol{r} \\ \delta\dot{\boldsymbol{r}} \\ \delta\boldsymbol{q}_{\boldsymbol{v}} \\ \delta\boldsymbol{\omega} \end{bmatrix} \tag{32}$$

$$\delta\dot{\boldsymbol{r}} = \delta\dot{\boldsymbol{r}} \tag{33}$$

$$\delta\dot{\boldsymbol{q}}_{\boldsymbol{v}} = \frac{1}{2}q_{ve}\times\delta\omega \tag{34}$$

$$\delta\ddot{\boldsymbol{r}} = a_{21}\delta\boldsymbol{r} + a_{23}\delta\boldsymbol{q}_{\boldsymbol{v}} \tag{35}$$

$$\delta\dot{\boldsymbol{\omega}} = a_{41}\delta\boldsymbol{r} + a_{43}\delta\boldsymbol{q}_{\boldsymbol{v}} \tag{36}$$

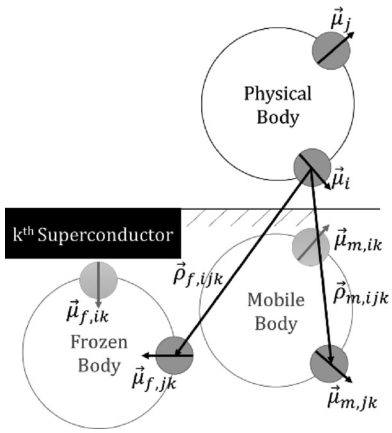

Fig. 4. Frozen and mobile images from magnet *j* acting on magnet *i* across superconductor *k*.

IV. Linearized Rigid Body Dynamics for an Arbitrary Number of Magnets and Superconductors

For a system of M rigidly constrained magnets on a rigid body with each magnet flux pinned to N fixed superconductors, each superconductor will store M frozen images. The system of permanent magnets will feel the effect of each Nth superconductor's embedded images, in which each superconductor holds M frozen images, totaling $M \times N$ frozen images. An equal number of mobile images pair with the frozen image counterparts, yielding a total $2 \times M \times N$ images that generate forces and torques. Assuming the magnets are rigidly mounted together, the summation of the forces on each magnet yields the total force on the body at the magnet bodies' center of mass.

A single flux-pinned interaction happens between the images of magnets i and j, in which magnet j produces frozen and mobile images on superconductor k, given by (41) and shown in Fig. 4. Magnet j produces frozen and mobile images on multiple superconductors, which all affect magnet i. The total contribution of magnet j's images onto magnet i is the summation of all individual flux-pinned interactions between magnets i and j across all superconductors, given by (42). The total force on magnet i from all magnet images is the sum of all magnet j influences across all superconductors, given by (43). The total force on a rigid body is the summation of total force on each magnet I, given by (44).

The torque is similar to the force summation with an extra term attributed to the force with a moment arm on magnet i, given by (45). The total torque on a rigid body is analogous to the total force equation but also includes a torque from each force displaced from the center of mass, given by (46). These two summation equations can be rearranged into a linear set of equations using the same linearization techniques from the single magnet single superconductor case.

$$\boldsymbol{F}_{ijk} = \boldsymbol{F}_{\mathbf{frozen}} + \boldsymbol{F}_{\mathbf{mobile}} \tag{41}$$

$$\boldsymbol{F}_{ij} = \sum_{k=1}^{M} (\boldsymbol{F}_{\mathbf{frozen}} + \boldsymbol{F}_{\mathbf{mobile}})_k \tag{42}$$

$$\boldsymbol{F}_{i} = \sum_{j=1}^{N}\sum_{k=1}^{M} ((\boldsymbol{F}_{\mathbf{frozen}} + \boldsymbol{F}_{\mathbf{mobile}})_k)_j \tag{43}$$

$$\boldsymbol{F}_{COM} = \sum_{i=1}^{N}\sum_{j=1}^{N}\sum_{k=1}^{M} \Big(((\boldsymbol{F}_{\mathbf{frozen}} + \boldsymbol{F}_{\mathbf{mobile}})_k)_j\Big)_i \tag{44}$$

$$\boldsymbol{\tau}_{i} = \sum_{j=1}^{N}\sum_{k=1}^{M} ((\boldsymbol{\tau}_{\mathbf{frozen}} + \boldsymbol{\tau}_{\mathbf{mobile}})_k)_j + \boldsymbol{\rho}_i \times \boldsymbol{F}_i \tag{45}$$

$$\boldsymbol{\tau}_{COM} = \sum_{i=1}^{N}\sum_{j=1}^{N}\sum_{k=1}^{M} \Big(((\boldsymbol{\tau}_{\mathbf{frozen}} + \boldsymbol{\tau}_{\mathbf{mobile}})_k)_j\Big)_i + \sum_{i=1}^{M} \boldsymbol{\rho}_i \times \boldsymbol{F}_i. \tag{46}$$

$$a_{21} = M^{-1}\frac{3\mu_0}{4\pi|\rho_e|^5}\begin{pmatrix} m_{fe}^{\times}m_e^{\times} + m_e^{\times}m_{fe}^{\times} - 2m_e^T m_{fe}\underline{1} - \frac{5}{|\rho_e|^2}\left(\rho_e\left(\rho_e^{\times}m_{fe}\right)^T m_e^{\times} - \rho_e\left(\rho_e^{\times}m_e\right)^T m_{fe}^{\times}\right) + \\ -\frac{5}{|\rho_e|^2}\left(\left(\rho_e^{\times}m_e\right)^{\times}m_{fe} + \left(\rho_e^{\times}m_{fe}\right)^{\times}m_e - 2\left(m_e^T m_{fe}\right)\rho_e + \frac{5}{|\rho_e|^2}\left(\left(\rho_e^{\times}m_e\right)^T\left(\rho_e^{\times}m_{fe}\right)\right)\rho_e^T\right) + \\ 2\hat{m}_s\hat{m}_s^T\Big(m_{me}^{\times}m_e^{\times} + m_e^{\times}m_{me}^{\times} - 2m_e^T m_{me}\underline{1} - \frac{5}{|\rho_e|^2}\left(\rho_e\left(\rho_e^{\times}m_{me}\right)^T m_e^{\times} - \rho_e\left(\rho_e^{\times}m_e\right)^T m_{me}^{\times}\right) \\ -\frac{5}{|\rho_e|^2}\left(\left(\rho_e^{\times}m_e\right)^{\times}m_{me} + \left(\rho_e^{\times}m_{me}\right)^{\times}m_e - 2\left(m_e^T m_{me}\right)\rho_e + \frac{5}{|\rho_e|^2}\left(\left(\rho_e^{\times}m_e\right)^T\left(\rho_e^{\times}m_{me}\right)\right)\rho_e^T\right)\Big) \end{pmatrix} \tag{37}$$

$$a_{23} = M^{-1}\frac{3\mu_0|m_e|}{4\pi|\rho_e|^5}\begin{pmatrix} -m_{fe}^{\times}\rho_e^{\times} + \left(\rho_e^{\times}m_{fe}\right)^{\times} - 2\rho_e m_{fe}^T + \frac{5}{|\rho_e|^2}\rho_e\left(\rho_e^{\times}m_{fe}\right)^T\rho_e^{\times} + \\ -m_{me}^{\times}\rho_e^{\times} + \left(\rho_e^{\times}m_{me}\right)^{\times} - 2\rho_e m_{me}^T + \frac{5}{|\rho_e|^2}\rho_e\left(\rho_e^{\times}m_{me}\right)^T\rho_e^{\times} + \\ \left(\underline{1} - 2\hat{m}_s\hat{m}_s^T\right)\left(\left(\rho_e m_e\right)^{\times} - m_e^{\times}\rho_e^{\times} - 2\rho_e m_e^T + \frac{5}{|\rho_e|^2}\rho_e\left(\rho_e^{\times}m_e\right)^T\rho_e^{\times}\right) \end{pmatrix} \tag{38}$$

$$a_{41} = I^{-1}\frac{\mu_0}{4\pi|\rho_e|^3}\begin{pmatrix} \frac{3}{|\rho_e|^2}\left(m_e^T\rho_e m_{fe}^{\times} + m_{fe}^T\rho_e m_e^{\times} - \left(\frac{3}{|\rho_e|^2}m_e^T\rho_e m_{fe}^{\times}\rho_e + m_e^{\times}m_{fe}\right)\rho_e^T\right) + \\ 2\hat{m}_s\hat{m}_s^T\left(\frac{3}{|\rho_e|^2}\left(m_e^T\rho_e m_{me}^{\times} + m_{me}^T\rho_e m_e^{\times} - \left(\frac{3}{|\rho_e|^2}m_e^T\rho_e m_{me}^{\times}\rho_e + m_e^{\times}m_{me}\right)\rho_e^T\right)\right) \end{pmatrix} \tag{39}$$

$$a_{43} = I^{-1}\frac{\mu_0|m_e|}{4\pi|\rho_e|^3}\left(\frac{3}{|\rho_e|^2}m_{fe}^{\times}\rho_e\rho_e^T - m_{fe}^{\times} + \frac{3}{|\rho_e|^2}m_{me}^{\times}\rho_e\rho_e^T - m_{me}^{\times} + \left(2\hat{m}_s\hat{m}_s^T - \underline{1}\right)\left(\frac{3}{|\rho_e|^2}m_e^{\times}\rho_e\rho_e^T + m_e^{\times}\right)\right). \tag{40}$$

The state space of the single magnet single superconductor case has 12 state variables: translational position, translational velocity, quaternion vector, and angular velocity of the magnet. For the general case of an M magnet N superconductor interaction, the states will include those 12 state variables for each magnet on the rigid body, i.e., $12M$ total states. The most general plant, given in (47), is a simplification of the multiple magnet and multiple superconductor plant to a matrix of block matrices, where $\delta z_i = [\delta \boldsymbol{r}_i \delta \dot{\boldsymbol{r}}_i \delta \boldsymbol{q}_{vi} \delta \boldsymbol{\omega}_i]^T$ and $A_{\mathrm{i,j}}$ is the linearized dynamics of magnet i due to magnet j's images.

$$\begin{bmatrix} \delta \dot{z}_1 \\ \vdots \\ \delta \dot{z}_m \end{bmatrix} = \begin{bmatrix} A_{1,1} & \cdots & A_{1,M} \\ \vdots & \ddots & \vdots \\ A_{M,1} & \cdots & A_{M,M} \end{bmatrix} \begin{bmatrix} \delta z_1 \\ \vdots \\ \delta z_m \end{bmatrix} \tag{47}$$

Four Jacobians provide the basis for the partitions in the $A_{i,j}$ matrix of (47): force and torque as a function of position and orientation. The single magnet and single superconductor plant is derived using this general form $A_{i,j}$, given by (48). The magnet images affecting the dynamics can be from any magnet's images embedded in any superconductor. Every interaction is pairwise and all block matrices are populated. The larger system variables are analogous to the single magnet and single superconductor variables in (33)–(40). The velocity of magnet i is only the velocity of magnet j, when $i = j$. The quaternion derivative of magnet i is only propagated when magnet $j = i$. Any magnetic moment dipole from an image is established from magnet j about superconductor k. Any magnetic moment dipole from a magnet is established from magnet i. The distance vectors are calculated from magnet j's images about superconductor k to magnet i. These equations constitute the entries of the linearized state matrix, forming the basis of a linearized flux-pinning dynamics model for magnet i from specific magnet j's images from superconductor k. $a_{21,ij}$, $a_{23,ij}$, $a_{41,ij}$, and $a_{43,ij}$ are expressions with summation over all N superconductors.

$$\begin{bmatrix} \delta \dot{\boldsymbol{r}}_i \\ \delta \ddot{\boldsymbol{r}}_i \\ \delta \dot{\boldsymbol{q}}_{vi} \\ \delta \dot{\boldsymbol{\omega}}_i \end{bmatrix} = A_{i,j} \begin{bmatrix} \delta \boldsymbol{r}_j \\ \delta \dot{\boldsymbol{r}}_j \\ \delta \boldsymbol{q}_{vj} \\ \delta \boldsymbol{\omega}_j \end{bmatrix} \tag{48}$$

where

$$A_{i,j} = \begin{bmatrix} 0 & a_{12,ij} & 0 & 0 \\ a_{21,ij} & 0 & a_{23,ij} & 0 \\ 0 & 0 & 0 & a_{34,ij} \\ a_{41,ij} & 0 & a_{43,ij} & 0 \end{bmatrix}.$$

The output states of a rigid body about the center of mass are translational position, translational velocity, attitude, and angular velocity of the magnet. For the M magnet N superconductor case, the input state includes the position, velocity, attitude, and angular velocity of every magnet j, where A_j represents the contribution to body dynamics from magnet j's state, given by (49). $a_{21,j}$, $a_{23,j}$, $a_{41,j}$, and $a_{43,j}$ are expressions with summation over all N superconductors and M magnets. An analogous operation would be to sum each $A_{i,j}$ block matrix along each column or ith index, resulting in A_j. These 3×3 block matrices form the basis of a linearized flux-pinning dynamics model for a rigid body with all M magnets.

$$\begin{bmatrix} \delta \dot{\boldsymbol{r}}_{COM} \\ \delta \ddot{\boldsymbol{r}}_{COM} \\ \delta \dot{\boldsymbol{q}}_{vCOM} \\ \delta \dot{\boldsymbol{\omega}}_{COM} \end{bmatrix} = \begin{bmatrix} A_1 & \ldots & A_M \end{bmatrix} \begin{bmatrix} \delta \boldsymbol{r}_1 \\ \delta \dot{\boldsymbol{r}}_1 \\ \delta \boldsymbol{q}_{v1} \\ \delta \boldsymbol{\omega}_1 \\ \vdots \\ \delta \boldsymbol{r}_m \\ \delta \dot{\boldsymbol{r}}_m \\ \delta \boldsymbol{q}_{vM} \\ \delta \boldsymbol{\omega}_m \end{bmatrix} \tag{49}$$

where

$$A_{i,j} = \begin{bmatrix} 0 & a_{12,ij} & 0 & 0 \\ a_{21,ij} & 0 & a_{23,ij} & 0 \\ 0 & 0 & 0 & a_{34,ij} \\ a_{41,ij} & 0 & a_{43,ij} & 0 \end{bmatrix}.$$

V. Sensitivity and Comparison of Single Magnet and Single Superconductor Dynamics

To validate the linearized dynamics and investigate the dynamic sensitivity of each state, a simulation with the full nonlinear dynamic equations is compared to the linearized state space. The fully nonlinear simulation also offers a second method to validate the linearized state space, using a common software package. Dynamic characteristics of the linearized state space are discussed, followed by a comparison of the nonlinear dynamic time histories and the derived linearized state-space-propagated dynamics to generate the RMS error. Finally, this paper studies the sensitivity of force and torque by independently varying each state.

A. *Defining System Parameters*

The specific magnet chosen is that of strength 0.8815 T and diameter 0.75 in. If z represents the vertical height in the Cartesian coordinate space, the magnet is field-cooled 1 cm above the superconductor. Both the superconductor and magnet are pointing directly upward. The position of the permanent magnet from an arbitrary origin on the superconductor surface is represented by $\boldsymbol{r}_1$. The magnetic moment dipole of the permanent magnet contains a field strength and a unit direction, represented by $\boldsymbol{m}_1$. The orientation of the superconductor is the surface normal unit vector, given by $\hat{\boldsymbol{m}}_s$. The mass matrix is the mass of the permanent magnet, multiplied by an identity matrix, given by M. R is the radius of the spherical magnetic moment dipole. I is the inertia tensor of the spherical magnet.

From these physical parameters, the image parameters are found. $\boldsymbol{r}_f$ is the position of the frozen image. $\boldsymbol{r}_m$ is the position of the mobile image. $\boldsymbol{\rho}_e$ is the position vector from the images

TABLE I
SINGLE MAGNET AND SUPERCONDUCTOR CASE STUDY PARAMETERS

Distance [m]	Magnet Moment Dipole [T]	Body Parameters
$\boldsymbol{r_1}$ = [0; 0; 0.01]	$\boldsymbol{m_1}$ = 0.8815[0; 0; 1]	$\widehat{m}_s$ = [0; 0; 1]
$\boldsymbol{\rho_e}$ = [0; 0; 0.02]	$\boldsymbol{m_e}$ = 0.8815[0; 0; 1]	M = 0.0272 kg
$\boldsymbol{r_f}$ = [0; 0; −0.01]	$\boldsymbol{m_{fe}}$ = 0.8815[0; 0; 1]	R = 0.009525m
$\boldsymbol{r_m}$ = [0; 0; −0.01]	$\boldsymbol{m_{me}}$ = 0.8815[0; 0; −1]	$I = 3.63 \times 10^{-5}$ kg-m^2

TABLE II
SINGLE MAGNET AND SUPERCONDUCTOR EIGENPAIRS

eigenpair	λ	mode	shape
1	108.5i	ω_y	$\dot{r}_x$
2	-108.5i	ω_y	$\dot{r}_x$
3	108.5i	ω_x	$\dot{r}_y$
4	-108.5i	ω_x	$\dot{r}_y$
5	37.4i	ω_x	ω_y
6	-37.4i	ω_x	ω_y
7	37.4i	ω_y	ω_x
8	-37.4i	ω_y	ω_x
9	146.4i	$\dot{r}_z$	r_z
10	-146.4i	$\dot{r}_z$	r_z
11	0	q_3	r_z
12	0	q_3	

to the permanent magnet when in equilibrium, which is also the field-cooled position. The equilibrium magnetic moment dipole is equivalent to the field-cooled orientation of the permanent magnet $\boldsymbol{m_e}$. The frozen-image magnetic moment dipole $\boldsymbol{m_{fe}}$ is of the same orientation as the permanent magnet orientation when field-cooled. The mobile image magnetic moment dipole $\boldsymbol{m_{me}}$ is the mirrored orientation as the permanent magnet orientation when field-cooled. Table I presents a complete list of system parameters. All code is online and available at github.com/frankiezoo/SMSS Linear Dynamics.git.

B. Linearizing a Nonlinear Simulation and Deriving Linearized Matrix

After building a nonlinear dynamics model of a single magnet and single superconductor, the model is linearized with the help of the Linear Analysis Toolbox from MathWorks Simulink. The input perturbation states are the quaternion and the position of the permanent magnet. The output measurement is the force and torque. The state space produced from Simulink's linearization produces (50). The single magnet and single superconductor plant from (32) is modified to include the four Jacobians from Simulink's linearization process from (49), given by (51). The state matrix generated from the simulation is equivalent within machine precision to the linearized state matrix derived in the preceding sections.

$$J = \begin{bmatrix} \frac{\partial \boldsymbol{F}}{\partial \boldsymbol{r}} & \frac{\partial \boldsymbol{F}}{\partial \boldsymbol{q}} \\ \frac{\partial \boldsymbol{\tau}}{\partial \boldsymbol{r}} & \frac{\partial \boldsymbol{\tau}}{\partial \boldsymbol{q}} \end{bmatrix} \tag{50}$$

$$\begin{bmatrix} \delta\dot{\boldsymbol{r}} \\ \delta\ddot{\boldsymbol{r}} \\ \delta\dot{\boldsymbol{q}}_{\boldsymbol{v}} \\ \delta\dot{\boldsymbol{\omega}} \end{bmatrix} = \begin{bmatrix} 0 & \underline{1} & 0 & 0 \\ M^{-1}\frac{\partial \boldsymbol{F}}{\partial \boldsymbol{r}} & 0 & M^{-1}\left|\boldsymbol{m}_e\right|\frac{\partial \boldsymbol{F}}{\partial \boldsymbol{q}} & 0 \\ 0 & 0 & 0 & \frac{1}{2}q_{ve}^{\times} \\ I^{-1}\frac{\partial \boldsymbol{\tau}}{\partial \boldsymbol{r}} & 0 & I^{-1}\left|\boldsymbol{m}_e\right|\frac{\partial \boldsymbol{\tau}}{\partial \boldsymbol{q}} & 0 \end{bmatrix} \begin{bmatrix} \delta\boldsymbol{r} \\ \delta\dot{\boldsymbol{r}} \\ \delta\boldsymbol{q}_{\boldsymbol{v}} \\ \delta\boldsymbol{\omega} \end{bmatrix}. \tag{51}$$

C. Modal Analysis of Linearized Flux-Pinned Model

Modal analysis of a dynamic system reveals stability and frequency information. The eigenvalues and eigenvectors are found with the linearized state-space matrix. The plant derived in Section V-B has the following eigenpairs. The flux-pinned system is marginally stable because all eigenvalues have a 0 real component. The numerical values associated with each eigenpair manifest different properties in the physical system, as shown in Table II.

The first ten eigenvalues of the flux-pinned plant are all imaginary, which represent the spring-like nature of flux-pinned interfaces. Due to the axial symmetry of the magnet, the eigenvalues representing the x and y dynamics come in quadruplets. The eigenvectors with imaginary values must be paired with the conjugate eigenvector to manifest real physical dynamics. Intuitively, flux-pinned interfaces have stiffer translational joints than rotational joints. The modal analysis reveals the same conclusion, where the z translation has the highest stiffness, the x and y translations are also relatively high, and the x and y rotations have the lowest stiffness.

The first four modes show a relation between the rotation and translation about the x and y axes. The rotation is the main modal shape, but contributes to the translation. This stiffness is rather high. The next four modes, 5–8, show a relation between the rotation about the x and y axes. The rotation about one axis is the main modal shape, but the rotation about the other axis is also a significant modal. This stiffness is the lowest of all modes. Modes 9 and 10 strictly reflect translation in the z direction. It has the highest stiffness of all the modes. The last modes have 0 eigenvalues because the dynamics of the system do not resist to any perturbation of these states. Any perturbation in q_3, or the magnetic strength of the magnet, results in translation in the z direction. Any perturbation in the rotation about the z-axis q_3 results in rotation about the z-axis until another perturbation or energy dissipation is introduced.

D. Sensitivity of Linearized Dynamics due to State Variation

Although the linearized plant is nearly exact to machine precision error at equilibrium, the linear plant approximates nonlinear dynamics less accurately the further the system deviates from equilibrium. Figs. 5–9 show sensitivity plots varying state variables and correlating error in force and torque calculations between the linearized equations and nonlinear equations. The translation and rotation in the x and y directions are the same due

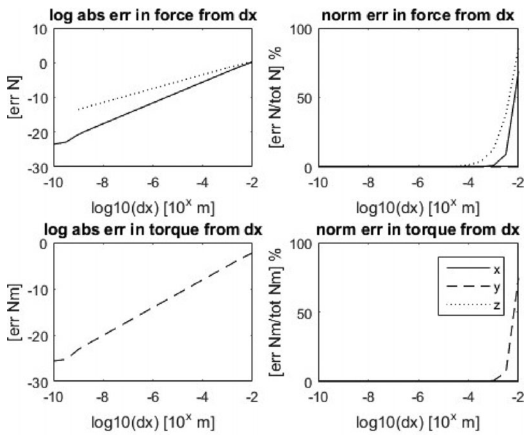

Fig. 5. Error in force and torque between linearized and nonlinear models when varying displacement along the *x* direction.

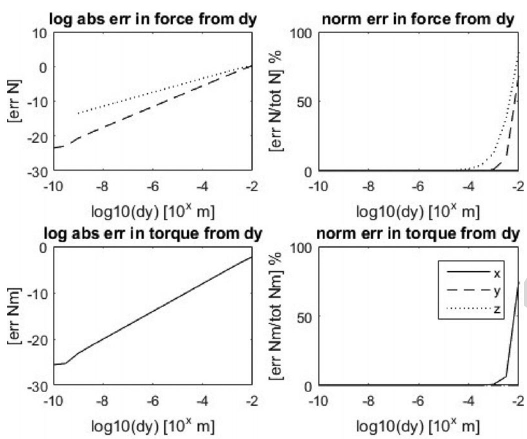

Fig. 6. Error in force and torque between linearized and nonlinear models when varying displacement along the *y* direction.

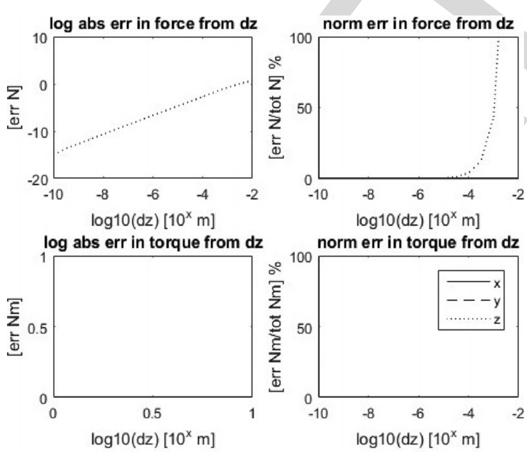

Fig. 7. Error in force and torque between linearized and nonlinear models when varying displacement along the *z* direction.

to symmetry, as shown in Figs. 5, 6, 8, and 9. There is no rotation in the *z* direction because the magnet is axially symmetric. The most sensitive state is the translational displacement in the *z* direction, as shown in Fig. 7. The equilibrium separation distance from the superconductor surface is 1 cm, or 10^{-2} m. To retain

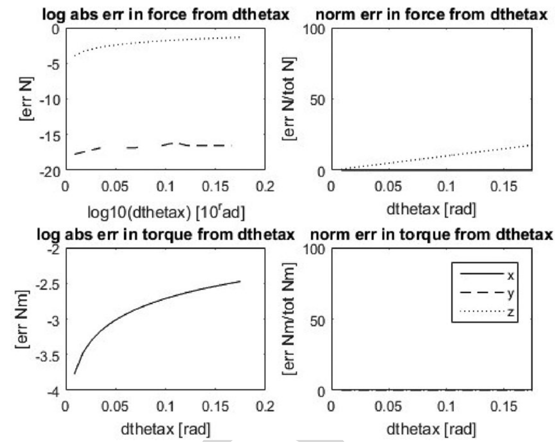

Fig. 8. Error in force and torque between linearized and nonlinear models when varying rotation along the *x* direction.

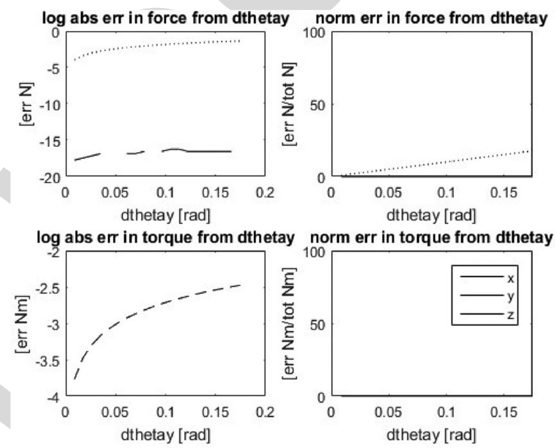

Fig. 9. Error in force and torque between linearized and nonlinear models when varying rotation along the *y* direction.

below 5% error in force, displacements in the *z* direction must be bound to 10^{-4} m. This requirement is much more stringent if the error threshold is 1%, decreasing the displacement bound down to 10^{-5} m. Perturbations in the *x* and *y* translational displacements may be as high as 1 m, or 10^{-3} m, yet still retaining 5% RMS error in force.

VI. Conclusion

The general, linearized state-space equations derived here allow the closed-form analytical characterization of a flux-pinned interface, along with the state matrix needed to formulate linear control algorithms. The results are an important step toward implementing six degree-of-freedom dynamic systems, such as docking, formation flying, autonomous assembly of multiple bodies, and noncontacting pointing platforms.

This model is expected to help characterize the passive dynamics of a flux-pinned system in all its degrees of freedom to permit the formulation of control algorithms. The linearized model accurately reflects the nonlinear dynamics within small displacements. Understanding the sensitivity of spatial perturbations informs the implementation of feedback control, for example, in choosing the proper sensor resolution and predicting the expected excursions of the flux-pinned interface dynamics.

Although the linearized equations are consistent with the fundamental physics, Kordyuk's geometric mapping and Villani's dipole interactions represent limitations that may come into play for systems with nonlinear excursions and for which the dipole assumptions break down. Future work lies in refining the basic nonlinear flux-pinning model and parameterizing the nonlinearities in the dynamics model.

References

[1] S. Earnshaw, "On the nature of the molecular forces which regulate the constitution of the luminiferous ether," *Trans. Camb. Philos. Soc.*, vol. 7, pp. 97–112, 1842.

[2] R. Williams and J. R. Matey, "Equilibrium of a magnet floating above a superconducting disk," *Appl. Phys. Lett.*, vol. 52, no. 9, pp. 751–753, Feb. 1988.

[3] C. Navau, N. Del-Valle, and A. Sanchez, "Macroscopic modeling of magnetization and levitation of hard type-II superconductors: The critical-state model," *IEEE Trans. Appl. Supercond.*, vol. 23, no. 1, Feb. 2013, Art. no. 8201023.

[4] A. A. Kordyuk, "Magnetic levitation for hard superconductors," *J. Appl. Phys.*, vol. 83, no. 1, pp. 610–612, Jan. 1998.

[5] F. Zhu, L. Jones-Wilson, and M. Peck, "Flux-pinned dynamics model parameterization and sensitivity study," presented at the IEEE Aerospace Conf., Big Sky, Montana, 2018.

[6] Y. Yang and X. Zheng, "Method for solution of the interaction between superconductor and permanent magnet," *J. Appl. Phys.*, vol. 101, no. 11, Jun. 2007, Art. no. 113922.

[7] K. W. Yung, P. B. Landecker, and D. D. Villani, "An analytic solution for the force between two magnetic dipoles," *Phys. Sep. Sci. Eng.*, vol. 101, no. 11, pp. 39–52, 1998.

[8] P. B. Landecker, D. D. Villani, and K. W. Yung, "An analytic solution for the torque between two magnetic dipoles," *Phys. Sep. Sci. Eng.*, vol. 10, no. 1, pp. 29–33, 1999.

[9] M. K. Alqadi, F. Y. Alzoubi, H. M. Al-khateeb, and N. Y. Ayoub, "Interaction between a point magnetic dipole and a high-temperature superconducting sphere," *Phys. B: Condens. Matter*, vol. 404, no. 12, pp. 1781–1784, Jun. 2009.

[10] A. Cansiz, J. R. Hull, and Ö. Gundogdu, "Translational and rotational dynamic analysis of a superconducting levitation system," *Supercond. Sci. Technol.*, vol. 18, no. 7, 2005, Art. no. 990.

[11] T. Sugiura, H. Ura, and K. Kuroda, "Magnetic stiffness of a coupled high-T_c superconducting levitation system," *Phys. C: Supercond.*, vol. 392, pp. 648–653, 2003.

[12] L. Jones and M. Peck, "Control strategies utilizing the physics of flux-pinned interfaces for spacecraft," in *Proc. AIAA Guidance, Navigation, Control Conf.*

[13] T. Chow, *Introduction to Electromagnetic Theory: A Modern Perspective*. Boston, MA, USA: Jones & Bartlett, 2006.

Frances Zhu received the B.S. degree in mechanical and aerospace engineering from Cornell University, Ithaca, NY, USA, in 2014, where she is currently working toward the Ph.D. degree in aerospace engineering.

Since 2014, she has been a Research Assistant with the Space Systems Design Studio, Ithaca, NY, USA, specializing in dynamics, systems, and controls engineering. Her research interests include flux-pinned interface applications, spacecraft system architectures, robot dynamics, estimation, and controls.

Ms. Zhu is a NASA Space Technology Research Fellow.

Mason A. Peck received the B.S. degree in aerospace engineering from the University of Texas at Austin, Austin, TX, USA, and the M.S. and Ph.D. degrees from the University of California, Los Angeles, Los Angeles, CA, USA, as a Howard Hughes Fellow from 1998 to 2001.

From 1993 to 1994, he worked at Bell Helicopter on structural dynamics. From 1994 to 2001, he was an Attitude Dynamics Specialist and Systems Engineer at Hughes Space and Communications (now Boeing Satellite Systems). During his years at Boeing, he served as Attitude Dynamics Lead in the Boeing Mission Control Center, participating in real-time spacecraft operations and helping to resolve spacecraft performance anomalies. In 2001, he joined Honeywell Defense and Space Systems, and in 2003 was named Principal Fellow. He has several patents on his name. In July 2004, he joined as a Faculty at Cornell University, where he teaches courses in dynamics and control and in the mechanical and aerospace engineering program, where he was promoted to an Associate Professor in fall 2010. In 2012, he was appointed as NASA's Chief Technologist.

GENERAL INSTRUCTION

- Authors: Please note that we cannot accept new source files as corrections for your paper. If possible, please annotate the PDF proof we have sent you with your corrections and upload it via the Author Gateway. Alternatively, you may send us your corrections in list format. You may also upload revised graphics via the Author Gateway.

QUERIES

Q1. Author: Fig. 1 is not cited in the text. Please cite it at an appropriate place.
Q2. Author: The word axis and direction has been added after x, y and z here and elsewhere in the text and figure captions. Please check for correctness.
Q3. Author: Please provide the page range for reference [12].
Q4. Author: Please mention the years in which Mason. A Peck received the B.S., M.S., and Ph.D. degrees.

Linearized Dynamics of General Flux-Pinned Interfaces

Frances Zhu and Mason A. Peck

***Abstract*—A flux-pinned interface offers a passively stable equilibrium that otherwise cannot occur between magnets because electromagnetic fields are divergenceless. The contactless, compliant nature of flux pinning offers many benefits for close-proximity robotic maneuvers, such as rendezvous, docking, and actuation. This paper derives the six degree-of-freedom linear dynamics about an equilibrium for any magnet/superconductor configuration. Linearized dynamics are well suited to predicting close-proximity maneuvers, provide insights into the character of the dynamic system, and are essential for linear control synthesis. The equilibria and stability of a flux-pinned interface are found using Villani's equations for magnetic dipoles. Kordyuk's frozen-image model provides the nonlinear flux-pinning response to these magnetic forces and torques, all of which are then linearized. Comparing simulation results of the nonlinear and linear dynamics shows the extent of the linear model's applicability. Nevertheless, these simple models offer computational speed and physical intuition that a nonlinear model does not.**

***Index Terms*—Dynamics, linear systems, magnetoelectric effects, superconducting magnets.**

I. Introduction

Earnshaw's theorem states that there is no stable stationary equilibrium for point charges that are solely held together by electrostatic forces [1]. Because they are also divergenceless, magnetic fields offer no stable equilibria except at the origin or at infinity. This is not the case for flux-pinned magnets, for which a stable equilibrium can exist for any number of magnets at arbitrary relative positions and orientations. Flux pinning a magnet to a superconductor creates an equilibrium, or minimum potential energy well, that stabilizes the magnet's position and orientation.

An external magnetic field excites current vortices within a superconductor, which is a material that carries current without resistance. Cooling a Type II superconductor to below its transition temperature in the presence of a magnetic field establishes permanent current vortices, which persist as long as the superconductor's temperature stays below this threshold. The flux-pinning effect influences the dynamics of kilogram-scale bodies out to about 10 cm of separation distance. The energy in the magnetic field determines the range.

In early empirical studies of flux pinning, Williams noticed potential curves that resemble a volcano, with a minimum at the center of the disc and a maximum near the edge [2]. He proposed a model consisting of a repulsive magnetic field source (the mobile image) superimposed upon an attractive magnetic field source (the frozen image).

There are two conventional methods to model the magnetization of the superconductor: Bean's critical-state model and Kordyuk's frozen-image model [3], [4]. The critical-state model is general but numerically intensive because it is based on a finite-element analysis of interactions among—ideally—infinitesimally small magnetization loops. The accuracy of Bean's model depends on the resolution of magnetization loops, which cannot be feasibly solved in real time for problems of practical interest. Kordyuk's advanced frozen-image model represents the position and orientation of the two images within the superconductor geometrically, an approach that yields drastically simpler and faster real-time representations for feedback-control architectures. The frozen-image model omits the effects from physical parameters such as temperature, material, and geometry, but these may be accounted for in a modified frozen-image model [5]. For simplicity, the following assumptions are made. Critical current density is assumed to be infinite. For familiar problems, this limitation has no practical effect. The induced magnetic field is greater than the first critical magnetic field—again, an issue that rarely arises in practical applications. The temperature is low enough that scaling and hysteretic effects are negligible, although Yang offered a method to incorporate elastic hysteresis [6]. These assumptions, as well as the previous ones, are readily accommodated in systems designed for analyzability. Kordyuk's model and the magnetic moment dipole model provide the foundation for many subsequent analytical assessments of flux-pinned dynamics and are the basis for the rest of this paper [7], [8].

Kordyuk created an analytical model to explain the image effects of flux pinning, known as the frozen-image model [4]. Kordyuk's geometric relation between magnet parameters and image parameters is graphically depicted in–Fig. 2 and further discussed in Section II. Other authors (Alqadi [9], Cansiz [10], Suguira [11], etc.) have written primarily about finding the potential fields of magnet/superconductor arrangements or the equilibria of magnet/superconductor arrangements in three or less degrees of freedom. This paper derives the most general case of six degrees of freedom.

Manuscript received August 8, 2017; revised April 5, 2018; accepted May 30, 2018. This work was supported in part by the NASA Space Technology Research Fellowship under Grant NNX15AP55H. This paper was recommended by Associate Editor Philippe J. Masson. *(Corresponding author: Frances Zhu.)*

The authors are with the Department of Mechanical and Aerospace Engineering, Cornell University, Ithaca, NY 14853 USA (e-mail: fz55@cornell.edu; mp336@cornell.edu).

Color versions of one or more of the figures in this paper are available online at http://ieeexplore.ieee.org.

Digital Object Identifier 10.1109/TASC.2018.2844375

Q1 Fig. 1. Cryocooled superconductor with a pinned permanent magnet suspended in gravity.

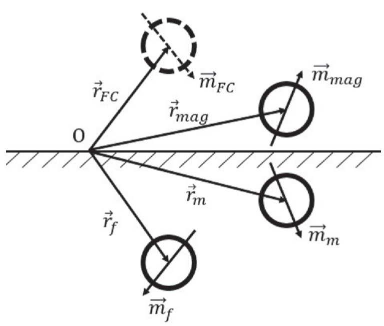

Fig. 2. Geometric relationship among the equilibrium, frozen image, mobile image, superconductor and magnet [4].

A flux-pinned interface offers many benefits for robotics applications, namely, passive stability, compliance, absence of mechanical contact, and low mass requirements. Flux-pinned systems can be actively manipulated to control the orientation and position of close-proximity vehicles while remaining contactless and compliant [12]. Traditional, linear control synthesis may be successful for such systems, but the inherently nonlinear dynamics must be linearized to provide a suitable plant model. A linearized model also provides valuable insights into the system, such as stability, natural frequencies, and modes. This study focuses on a general, linear model for these reasons.

II. Magnetic Field Sources

The general expression for magnetic field strength at distance $\boldsymbol{\rho}$ from the field source is (1) [10]. $\boldsymbol{m}$ is the magnetic moment of the dipole of interest. From (1), the magnetic field strength decreases with distance cubed. The expression for magnetic field strength can be related to a flux-pinned mobile image, flux-pinned frozen image, electromagnet, or permanent magnet. The magnetic field is a function of two variables: $\boldsymbol{m}$ the magnetic moment dipole and $\boldsymbol{\rho}$ the distance from the field source. $\boldsymbol{m}$ is a parameter determined by the physical nature of the source. $\boldsymbol{\rho}$ can be defined or measured in the physical system. The expression for magnetic moment dipoles differs for each type magnetic field source.

$$\boldsymbol{B}(\boldsymbol{\rho}) = \frac{\mu_0}{4\pi|\boldsymbol{\rho}|^3}\left(3\left(\boldsymbol{m}\cdot\hat{\boldsymbol{\rho}}\right)\hat{\boldsymbol{\rho}} - \hat{\boldsymbol{m}}\right). \tag{1}$$

A. Physical Magnet

There are two types of physical magnetic field sources: permanent magnets and electromagnets. The magnetic moment dipole of a permanent magnet is purely defined by physical characteristics in (2). B_0 is the manufacturer's measurement of the magnetic field at the surface of the magnet. d is the distance from the center of dipole to the surface. $\hat{\boldsymbol{m}}_{\boldsymbol{p}}$ is the unit direction of the magnetic moment dipole. The electromagnetic moment dipole is represented by (3), where $V(t)$ is the voltage potential of the electromagnet, A is the area enclosed by the electromagnet's coil of wire, T is the number of turns of the electromagnet, and R is the resistance of the electromagnet. Besides their physical differences, they mathematically represent a physical magnetic moment dipole $\boldsymbol{m}_{\boldsymbol{p}}$. Fig. 3(a) graphically depicts the relationship among variables. The two physical magnetic field sources differ in the physical parameters that make up the magnetic moment dipole expression.

$$\boldsymbol{m}_{\boldsymbol{p}} = \frac{2\pi B_0 d^3}{\mu_0}\hat{\boldsymbol{m}}_{\boldsymbol{p}} \tag{2}$$

$$\boldsymbol{m}_{\boldsymbol{E}} = \frac{VAT}{R}\hat{\boldsymbol{m}}_{\boldsymbol{E}}. \tag{3}$$

B. Mobile/Diamagnetic Image

All superconductors display the Meissner effect, which is the expulsion of magnetic flux. The magnetic source that creates the Meissner effect may be represented as an image within the superconductor that changes the polarity and magnitude to always repel. That image, more specifically, follows the external magnetic source and reorients to the moment dipole to mirror the external magnetic source. The mobile image's magnetic moment dipole depends on the permanent magnet's moment dipole and the orientation of the superconductor, given by (4). $\boldsymbol{m}_{\boldsymbol{mag}}$ is the vector from (2) or (3) that represents the physical magnet's moment dipole. $\hat{\boldsymbol{m}}_{\boldsymbol{s}}$ is the unit direction normal to the surface of the superconductor, illustrated in Fig. 3(b). The mobile image moves when the permanent magnet moves, so the location of the magnetic field from the mobile image is dynamic. $\boldsymbol{r}_{\boldsymbol{mag}}$ and $\boldsymbol{r}_{\boldsymbol{m}}$ change in the expression for magnetic field and potential energy, respectively. The magnetic field of the magnet's mobile image from Fig. 3(b) is given by (5), where $\boldsymbol{\rho}_{\boldsymbol{m}}$ is the distance from the mobile image to the permanent magnet that is given by (6), where $\boldsymbol{r}_{\boldsymbol{m}}$ is the location of the mobile image and $\boldsymbol{O}_{\boldsymbol{s}}$ is a point on the superconductor surface. The mobile image's magnetic moment dipole location and orientation are dependent on the superconductor's geometry.

$$\boldsymbol{m}_{\boldsymbol{m}} = \boldsymbol{m}_{\boldsymbol{mag}} - 2\left(\hat{\boldsymbol{m}}_s \cdot \boldsymbol{m}_{\boldsymbol{mag}}\right)\hat{\boldsymbol{m}}_s \tag{4}$$

$$\boldsymbol{\rho}_{\boldsymbol{m}} = \boldsymbol{r}_{\boldsymbol{mag}} - \boldsymbol{r}_{\boldsymbol{m}} \tag{5}$$

$$\boldsymbol{r}_{\boldsymbol{m}} = \boldsymbol{r}_{\boldsymbol{mag}} - 2\left(\left(\boldsymbol{r}_{\boldsymbol{mag}} - \boldsymbol{O}_s\right)\cdot\hat{\boldsymbol{m}}_s\right)\hat{\boldsymbol{m}}_s. \tag{6}$$

C. Physical Magnet

The frozen image is an image specific to high temperature or Type II superconductors. Instead of expelling all magnetic

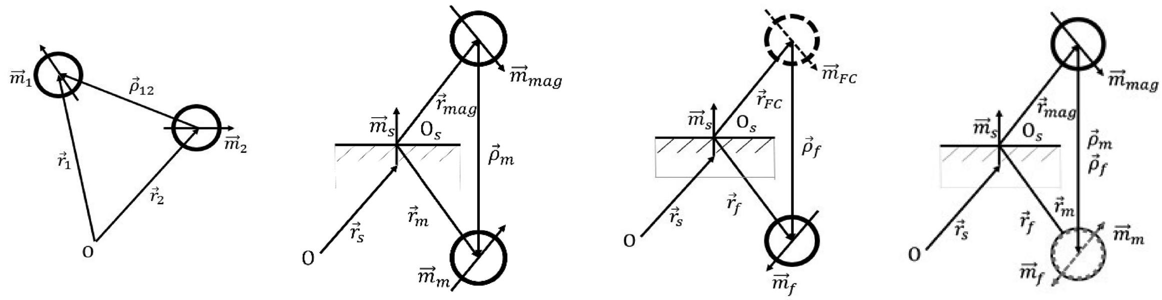

Fig. 3. Different types of magnetic field interactions. (a) Geometric representation of permanent magnet or electromagnet magnetic field source positions. (b) Geometric representation of mobile image magnetic field source positions. (c) Geometric representation of frozen-image magnetic field source positions. (d) Geometric representation of frozen image and mobile image overlaid at field-cooled position.

flux like Type I superconductors do, Type II superconductors field-cool a magnetic field during a transition phase and expel external fields that differ from the embedded field. This property allows for the stable presence of a field, in this application, infinitesimal magnetic dipole. The frozen image is a consequence of the presence of an infinitesimal magnetic dipole *a priori* and *a posteriori* cryocooling, which embeds a field in the superconductor that enforces restoration to this initial state. To counter the mobile image's repulsion, the frozen image acts as an attractive infinitesimal magnetic dipole that stays in place and aligns magnetic moment dipoles with the field-cooled magnet. The frozen image's magnetic moment dipole depends on the magnetic moment dipole field-cooled onto the superconductor and the orientation of the superconductor, as shown in (7) and geometrically in Fig. 3(c). Equations (8) and (9) are analogous to the frozen-image distance vectors. Like the mobile image, the frozen image is dependent on the superconductor's geometry, but, unlike the mobile image, it does not move when the permanent magnet moves after field cooling.

$$\boldsymbol{m}_f = 2\left(\hat{\boldsymbol{m}}_s \cdot \boldsymbol{m}_{FC}\right)\hat{\boldsymbol{m}}_s - \boldsymbol{m}_{FC} \tag{7}$$

$$\boldsymbol{\rho}_f = \boldsymbol{r}_{FC} - \boldsymbol{r}_f \tag{8}$$

$$\boldsymbol{r}_f = \boldsymbol{r}_{FC} - 2\left(\left(\boldsymbol{r}_{FC} - \boldsymbol{O}_s\right)\cdot\hat{\boldsymbol{m}}_s\right)\hat{\boldsymbol{m}}_s. \tag{9}$$

III. Linearized Dynamics for a Single Flux-Pinned Magnet and Superconductor Interaction

The linearized dynamics for the simplest flux-pinned interface is derived. The dynamics are solely dependent on the magnetic field source's position and orientation, along with physical parameters specific to the system geometry. Each subsection describes the linearization process briefly before presenting the final linearized equation set.

A. Linearizing General Magnetic Dipole Force and Torque Equations

Villani derived the force of a magnetic dipole $\boldsymbol{m_b}$ acting on another magnetic dipole $\boldsymbol{m_a}$ at distance $\boldsymbol{\rho}$, given by (10) shown at the bottom of this page, in which the scalars are brought out front and all vectors are unit direction vectors [4]. The final linearized force equation relates the first-order terms $\delta\boldsymbol{F_{ab}}$ to $\delta\boldsymbol{r}$, $\delta\boldsymbol{m_a}$, and $\delta\boldsymbol{m_b}$, all vectors denoting deviation from equilibrium. To linearize about $\boldsymbol{\rho_e}$, $\boldsymbol{m_{ae}}$, and $\boldsymbol{m_{be}}$, a first-order Taylor expansion of (10) was taken by replacing $\boldsymbol{F_{ab}} = \boldsymbol{F_e} + \delta\boldsymbol{F_{ab}}$, $\boldsymbol{\rho} = \boldsymbol{\rho_e} + \delta\boldsymbol{r}$, $\boldsymbol{m_a} = \boldsymbol{m_{ae}} + \delta\boldsymbol{m_a}$, and $\boldsymbol{m_b} = \boldsymbol{m_{be}} + \delta\boldsymbol{m_b}$. The equilibrium force is subtracted from both sides. The cross products and dot products are replaced with cross and transpose operators ($v\times$ to $v^\times$ and $v\cdot$ to v^T), and then rearranged to isolate the first-order terms. To transform the linear equation to matrix form, notice that the quantities in front of $\delta\boldsymbol{r}$, $\delta\boldsymbol{m_a}$, and $\delta\boldsymbol{m_b}$ are 3 $\times$ 3 matrices. The final matrix expression for linearized force between two magnetic moment dipoles is given by (11) shown at the bottom of this page. The moment/torque of a magnetic dipole $\boldsymbol{m_b}$ acting on another magnetic dipole $\boldsymbol{m_a}$ at distance ρ is given by (12), shown at the top of the next page, also derived by Villani [5]. The same process of linearization is applied to Villani's moment equation to yield (13) shown at the top of the next page.

B. Linearized Forces and Torques for Flux-Pinned Forces and Torques

The total force from a flux-pinned interaction is the superposition of the mobile image force and frozen-image force. These

$$\boldsymbol{F_{ab}} = \frac{3\mu_0 m_a m_b}{4\pi\rho^4}\left(\left(\hat{\boldsymbol{\rho}}\times\hat{\boldsymbol{m}}_{\boldsymbol{a}}\right)\times\hat{\boldsymbol{m}}_{\boldsymbol{b}} + \left(\hat{\boldsymbol{\rho}}\times\hat{\boldsymbol{m}}_{\boldsymbol{b}}\right)\times\hat{\boldsymbol{m}}_{\boldsymbol{a}} - 2\hat{\boldsymbol{\rho}}\left(\hat{\boldsymbol{m}}_{\boldsymbol{a}}\cdot\hat{\boldsymbol{m}}_{\boldsymbol{b}}\right) + 5\hat{\boldsymbol{\rho}}\left(\left(\hat{\boldsymbol{\rho}}\times\hat{\boldsymbol{m}}_{\boldsymbol{a}}\right)\cdot\left(\hat{\boldsymbol{\rho}}\times\hat{\boldsymbol{m}}_{\boldsymbol{b}}\right)\right)\right) \tag{10}$$

$$\delta\boldsymbol{F_{ab}} = \frac{3\mu_0}{4\pi|\rho_e|^5}\begin{bmatrix} m_{be}^\times m_{ae}^\times + m_{ae}^\times m_{be}^\times - 2m_{ae}^T m_{be}\underline{1} - \frac{5}{|\rho_e|^2}\left(\rho_e\left(\rho_e^\times m_{be}\right)^T m_{ae}^\times - \rho_e\left(\rho_e^\times m_{ae}\right)^T m_{be}^\times\right) + \cdots \\ -\frac{5}{|\rho_e|^2}\left(\left(\left(\rho_e^\times m_{ae}\right)^\times m_{be} + \left(\rho_e^\times m_{be}\right)^\times m_{ae} - 2\left(m_{ae}^T m_{be}\right)\rho_e + \frac{5}{|\rho_e|^2}\left(\left(\rho_e^\times m_{ae}\right)^T\left(\rho_e^\times m_{be}\right)\right)\right)\rho_e^T\right) \\ -m_{be}^\times\rho_e^\times + \left(\rho_e^\times m_{be}\right)^\times - 2\rho_e m_{be}^T + \frac{5}{|\rho_e|^2}\rho_e\left(\rho_e^\times m_{be}\right)^T\rho_e^\times \\ \left(\rho_e m_{ae}\right)^\times - m_{ae}^\times\rho_e^\times - 2\rho_e m_{ae}^T + \frac{5}{|\rho_e|^2}\rho_e\left(\rho_e^\times m_{ae}\right)^T\rho_e^\times \end{bmatrix}^T \begin{bmatrix}\delta\boldsymbol{r}\\ \delta\boldsymbol{m_a}\\ \delta\boldsymbol{m_b}\end{bmatrix} \tag{11}$$

$$\boldsymbol{\tau_{ab}} = \frac{\mu_0 m_a m_b}{4\pi\rho^3}\left(3\left(\boldsymbol{\hat{m}_a}\cdot\boldsymbol{\hat{\rho}}\right)\left(\boldsymbol{\hat{m}_b}\times\boldsymbol{\hat{\rho}}\right) + \left(\boldsymbol{\hat{m}_a}\times\boldsymbol{\hat{m}_b}\right)\right) \tag{12}$$

$$\delta\boldsymbol{\tau_{ab}} = \frac{\mu_0}{4\pi|\rho_e|^3}\begin{bmatrix} \frac{3}{|\rho_e|^2}\left(m_{ae}^T\rho_e m_{be}^\times + m_{be}^T\rho_e m_{ae}^\times - \left(\frac{3}{|\rho_e|^2}m_{ae}^T\rho_e m_{be}^\times\rho_e + m_{ae}^\times m_{be}\right)\rho_e^T\right) \\ \frac{3}{|\rho_e|^2}m_{be}^\times\rho_e\rho_e^T - m_{be}^\times \\ -\frac{3}{|\rho_e|^2}m_{ae}^\times\rho_e\rho_e^T - m_{ae}^\times \end{bmatrix}\begin{bmatrix}\delta\boldsymbol{r}\\ \delta\boldsymbol{m_a}\\ \delta\boldsymbol{m_b}\end{bmatrix}. \tag{13}$$

images are magnetic field sources that impart linearized forces given by (11). The frozen-image force is found by substituting $\boldsymbol{m_{ae}}$ to $\boldsymbol{m_e}$, the magnet's equilibrium magnetic moment dipole, and $\boldsymbol{m_{be}}$ to $\boldsymbol{m_{fe}}$, the frozen image's equilibrium magnetic moment dipole, into (11). The frozen image will never change in orientation; thus, $\delta\boldsymbol{m_f} = 0$. The linearized force from the frozen image is given by (14) shown at the bottom of this page. The mobile image force, given by (16), is similarly obtained by substituting $\boldsymbol{m_{ae}}$ to $\boldsymbol{m_e}$, the magnet's equilibrium magnetic moment dipole, and $\boldsymbol{m_{be}}$ to $\boldsymbol{m_{me}}$, the mobile image's equilibrium magnetic moment dipole, into (11). From Kordyuk's geometric interpretation of the frozen-image model, the mobile image reorients itself like a mirror image across the superconductors surface, where $\boldsymbol{\hat{m}_s}$ is the unit normal to the superconductor's surface given by (4). A direct relation from $\boldsymbol{m}$ to $\boldsymbol{m_m}$ is given by (15) shown at the bottom of this page. This relationship reduces the number of independent state variables. The mobile image force equation depends only on the magnet's orientation and position, given by (16) shown at the bottom of this page. The forces from the mobile and frozen images are additive and may be combined to a final equation for force on the system, given by (17) shown at the bottom of this page. The total force is dependent on the physical magnet's position and orientation, which constitutes the translational dynamic state of the flux-pinned interaction.

The total torque from a flux-pinned interface is the sum of the combined frozen and mobile image effects. The frozen-image torque is obtained by substituting $\boldsymbol{m_{ae}}$ to $\boldsymbol{m_e}$, the magnet's equilibrium magnetic moment dipole, and $\boldsymbol{m_{be}}$ to $\boldsymbol{m_{fe}}$, the frozen image's equilibrium magnetic moment dipole. The orientation of the frozen image does not change, so the state $\delta\boldsymbol{m_f}$ and the corresponding coefficient are excluded, given by (18) shown at the top of the next page. The same process is applied to the mobile image. Substituting (15) into our previous equation, we

$$\delta\boldsymbol{F_f} = \frac{3\mu_0}{4\pi|\rho_e|^5}\begin{bmatrix} m_{fe}^\times m_e^\times + m_e^\times m_{fe}^\times - 2m_e^T m_{fe}\underline{1} - \frac{5}{|\rho_e|^2}\left(\rho_e\left(\rho_e^\times m_{fe}\right)^T m_e^\times - \rho_e\left(\rho_e^\times m_e\right)^T m_{fe}^\times\right) + \cdots \\ -\frac{5}{|\rho_e|^2}\left(\left(\rho_e^\times m_e\right)^\times m_{fe} + \left(\rho_e^\times m_{fe}\right)^\times m_e - 2\left(m_e^T m_{fe}\right)\rho_e + \frac{5}{|\rho_e|^2}\left(\left(\rho_e^\times m_e\right)^T\left(\rho_e^\times m_{fe}\right)\right)\rho_e^T\right) \\ -m_{fe}^\times\rho_e^\times + \left(\rho_e^\times m_{fe}\right)^\times - 2\rho_e m_{fe}^T + \frac{5}{|\rho_e|^2}\rho_e\left(\rho_e^\times m_{fe}\right)^T\rho_e^\times \end{bmatrix}^T \begin{bmatrix}\delta\boldsymbol{r}\\ \delta\boldsymbol{m}\end{bmatrix} \tag{14}$$

$$\boldsymbol{m_m} = \left(\underline{1} - 2\boldsymbol{\hat{m}_s}\boldsymbol{\hat{m}_s^T}\right)\boldsymbol{m} \tag{15}$$

$$\delta\boldsymbol{F_m} = \frac{3\mu_0}{4\pi|\rho_e|^5}\begin{bmatrix} 2\hat{m}_s\hat{m}_s^T\left(m_{me}^\times m_e^\times + m_e^\times m_{me}^\times - 2m_e^T m_{me}\underline{1} - \frac{5}{|\rho_e|^2}\left(\rho_e\left(\rho_e^\times m_{me}\right)^T m_e^\times - \rho_e\left(\rho_e^\times m_e\right)^T m_{me}^\times\right) + \cdots \\ -\frac{5}{|\rho_e|^2}\left(\left(\rho_e^\times m_e\right)^\times m_{me} + \left(\rho_e^\times m_{me}\right)^\times m_e - 2\left(m_e^T m_{me}\right)\rho_e + \frac{5}{|\rho_e|^2}\left(\left(\rho_e^\times m_e\right)^T\left(\rho_e^\times m_{me}\right)\right)\rho_e^T\right)\right) \\ -m_{me}^\times\rho_e^\times + \left(\rho_e^\times m_{me}\right)^\times - 2\rho_e m_{me}^T + \frac{5}{|\rho_e|^2}\rho_e\left(\rho_e^\times m_{me}\right)^T\rho_e^\times + \cdots \\ \left(\underline{1} - 2\hat{m}_s\hat{m}_s^T\right)\left(\left(\rho_e m_e\right)^\times - m_e^\times\rho_e^\times - 2\rho_e m_e^T + \frac{5}{|\rho_e|^2}\rho_e\left(\rho_e^\times m_e\right)^T\rho_e^\times\right) \end{bmatrix}^T \begin{bmatrix}\delta\boldsymbol{r}\\ \delta\boldsymbol{m}\end{bmatrix} \tag{16}$$

$$\delta\boldsymbol{F_{tot}} = \frac{3\mu_0}{4\pi|\rho_e|^5}\begin{bmatrix} m_{fe}^\times m_e^\times + m_e^\times m_{fe}^\times - 2m_e^T m_{fe}\underline{1} - \frac{5}{|\rho_e|^2}\left(\rho_e\left(\rho_e^\times m_{fe}\right)^T m_e^\times - \rho_e\left(\rho_e^\times m_e\right)^T m_{fe}^\times\right) + \cdots \\ -\frac{5}{|\rho_e|^2}\left(\left(\rho_e^\times m_e\right)^\times m_{fe} + \left(\rho_e^\times m_{fe}\right)^\times m_e - 2\left(m_e^T m_{fe}\right)\rho_e + \frac{5}{|\rho_e|^2}\left(\left(\rho_e^\times m_e\right)^T\left(\rho_e^\times m_{fe}\right)\right)\rho_e^T\right) + \cdots \\ 2\hat{m}_s\hat{m}_s^T\left(m_{me}^\times m_e^\times + m_e^\times m_{me}^\times - 2m_e^T m_{me}\underline{1} - \frac{5}{|\rho_e|^2}\left(\rho_e\left(\rho_e^\times m_{me}\right)^T m_e^\times - \rho_e\left(\rho_e^\times m_e\right)^T m_{me}^\times\right) + \cdots \\ -\frac{5}{|\rho_e|^2}\left(\left(\rho_e^\times m_e\right)^\times m_{me} + \left(\rho_e^\times m_{me}\right)^\times m_e - 2\left(m_e^T m_{me}\right)\rho_e + \frac{5}{|\rho_e|^2}\left(\left(\rho_e^\times m_e\right)^T\left(\rho_e^\times m_{me}\right)\right)\rho_e^T\right)\right) \\ -m_{fe}^\times\rho_e^\times + \left(\rho_e^\times m_{fe}\right)^\times - 2\rho_e m_{fe}^T + \frac{5}{|\rho_e|^2}\rho_e\left(\rho_e^\times m_{fe}\right)^T\rho_e^\times + \cdots \\ -m_{me}^\times\rho_e^\times + \left(\rho_e^\times m_{me}\right)^\times - 2\rho_e m_{me}^T + \frac{5}{|\rho_e|^2}\rho_e\left(\rho_e^\times m_{me}\right)^T\rho_e^\times + \cdots \\ \left(\underline{1} - 2\hat{m}_s\hat{m}_s^T\right)\left(\left(\rho_e m_e\right)^\times - m_e^\times\rho_e^\times - 2\rho_e m_e^T + \frac{5}{|\rho_e|^2}\rho_e\left(\rho_e^\times m_e\right)^T\rho_e^\times\right) \end{bmatrix}^T \begin{bmatrix}\delta\boldsymbol{r}\\ \delta\boldsymbol{m}\end{bmatrix}. \tag{17}$$

$$\delta\boldsymbol{\tau}_{\boldsymbol{f}} = \frac{\mu_0}{4\pi|\rho_e|^3}\begin{bmatrix} \frac{3}{|\rho_e|^2}\left(m_e^T\rho_e m_{fe}^\times + m_{fe}^T\rho_e m_e^\times - \left(\frac{3}{|\rho_e|^2}m_e^T\rho_e m_{fe}^\times\rho_e + m_e^\times m_{fe}\right)\rho_e^T\right) \\ \frac{3}{|\rho_e|^2}m_{fe}^\times\rho_e\rho_e^T - m_{fe}^\times \end{bmatrix}^T \begin{bmatrix}\delta\boldsymbol{r} \\ \delta\boldsymbol{m}\end{bmatrix} \tag{18}$$

$$\delta\boldsymbol{\tau}_{\boldsymbol{m}} = \frac{\mu_0}{4\pi|\rho_e|^3}\begin{bmatrix} 2\hat{m}_s\hat{m}_s^T\left(\frac{3}{|\rho_e|^2}\left(m_e^T\rho_e m_{me}^\times + m_{me}^T\rho_e m_e^\times - \left(\frac{3}{|\rho_e|^2}m_e^T\rho_e m_{me}^\times\rho_e + m_e^\times m_{me}\right)\rho_e^T\right)\right) \\ \frac{3}{|\rho_e|^2}m_{me}^\times\rho_e\rho_e^T - m_{me}^\times + \left(2\hat{m}_s\hat{m}_s^T - \underline{1}\right)\left(\frac{3}{|\rho_e|^2}m_e^\times\rho_e\rho_e^T + m_e^\times\right) \end{bmatrix}^T \begin{bmatrix}\delta r \\ \delta m\end{bmatrix} \tag{19}$$

$$\delta\boldsymbol{\tau}_{\boldsymbol{tot}} = \frac{\mu_0}{4\pi|\rho_e|^3}\begin{bmatrix} \frac{3}{|\rho_e|^2}\left(m_e^T\rho_e m_{fe}^\times + m_{fe}^T\rho_e m_e^\times - \left(\frac{3}{|\rho_e|^2}m_e^T\rho_e m_{fe}^\times\rho_e + m_e^\times m_{fe}\right)\rho_e^T\right) + \cdots \\ 2\hat{m}_s\hat{m}_s^T\left(\frac{3}{|\rho_e|^2}\left(m_e^T\rho_e m_{me}^\times + m_{me}^T\rho_e m_e^\times - \left(\frac{3}{|\rho_e|^2}m_e^T\rho_e m_{me}^\times\rho_e + m_e^\times m_{me}\right)\rho_e^T\right)\right) \\ \frac{3}{|\rho_e|^2}m_{fe}^\times\rho_e\rho_e^T - m_{fe}^\times + \frac{3}{|\rho_e|^2}m_{me}^\times\rho_e\rho_e^T - m_{me}^\times + \left(2\hat{m}_s\hat{m}_s^T - \underline{1}\right)\left(\frac{3}{|\rho_e|^2}m_e^\times\rho_e\rho_e^T + m_e^\times\right) \end{bmatrix}^T \begin{bmatrix}\delta\boldsymbol{r} \\ \delta\boldsymbol{m}\end{bmatrix}. \tag{20}$$

reduce the number of states needed to calculate $\delta\boldsymbol{m}_{\boldsymbol{m}}$ given by (19) shown at the top of the next page. The total torque on the magnet is the sum of the torque from the mobile and frozen images, given by (20) shown at the top of this page. The total torque is solely dependent on the physical magnet's position and orientation, which constitutes the rotational dynamic state of the flux-pinned interaction.

C. Governing Equations

For the case of a single magnet and single superconductor, the magnet's dynamics are due to the forces and torques from the frozen and mobile images. In this single magnet case, there are two magnet moment dipoles that are exerting forces and torques on the magnet. The force and torque equations are given by (21) and (22), respectively. The translational dynamics of the flux-pinned magnet is a result of the force balance equation (23). The linear momentum balance, given by (24), is put into matrix form to be easily inserted into a state-space form later. Euler's rigid body equation (25) propagates attitude dynamics. The linearized version of the rigid body equations is given by (26). Equation (27) simplifies to no longer include the gyroscopic dynamics because the magnitude of angular velocity at equilibrium is 0. The orientation of the magnet may be represented by an Euler axis-angle (28), and alternatively by a quaternion (29). In this case, the Euler axis is the magnetic moment dipole unit vector, and the angle may be chosen to be π because the magnet is axisymmetric. Choosing π retains most of the information about the magnetic moment dipole-pointing vector. Upon inspection, the fourth component of the quaternion about equilibrium will always be zero; thus, no information is lost if the quaternion state vector is shortened to just the vector components q_v. To propagate the attitude dynamics, there is a linear relation between the quaternion and angular velocity that yields the quaternion derivative, given by (30). This set of equations fully defines the linearized dynamics of a rigid body.

$$\sum \boldsymbol{F} = \boldsymbol{F}_f + \boldsymbol{F}_{\boldsymbol{m}} \tag{21}$$

$$\sum \boldsymbol{\tau} = \boldsymbol{\tau}_f + \boldsymbol{\tau}_{\boldsymbol{m}} \tag{22}$$

$$\sum \boldsymbol{F} = M\ddot{\boldsymbol{r}} \tag{23}$$

$$\delta\ddot{\boldsymbol{r}} = \boldsymbol{M}^{-1}\delta\boldsymbol{F}_{\boldsymbol{tot}} \tag{24}$$

$$\boldsymbol{\tau} = I\cdot\dot{\boldsymbol{\omega}} + \boldsymbol{\omega}\times(I\cdot\boldsymbol{\omega}) \tag{25}$$

$$\delta\dot{\omega} = I^{-1}\left(\omega_e^\times I - (I\omega_e)^\times\right)\delta\omega + I^{-1}\tau \tag{26}$$

$$\delta\dot{\omega} = I^{-1}\delta\tau \tag{27}$$

$$\delta\boldsymbol{m} = \theta\delta\hat{\boldsymbol{m}} \tag{28}$$

$$\delta q = \begin{bmatrix}\delta\hat{\boldsymbol{m}}\sin\left(\frac{\theta}{2}\right) \\ \cos\left(\frac{\theta}{2}\right)\end{bmatrix} \tag{29}$$

$$\delta\dot{\boldsymbol{q}}_{\boldsymbol{v}} = \frac{1}{2}\boldsymbol{q}_{\boldsymbol{ve}}\times\delta\boldsymbol{\omega}. \tag{30}$$

D. State-Space Model

The single magnet flux-pinned system dynamics may be represented with a first-order system state-space matrix, given by (31). The state matrix has the form given in (32). Each entry in the state matrix is a block matrix of size corresponding to the state and resultant, where the following a_{ij} values are given by (34)–(40). The matrix entries a_{ij} are block matrices of size 3 × 3 that are generated from the linearized forces and torques from (17) and (20), respectively. Eq. (37)."(40) shown at the bottom of the next page.

$$\begin{bmatrix}\delta\dot{\boldsymbol{r}} \\ \delta\ddot{\boldsymbol{r}} \\ \delta\dot{\boldsymbol{q}}_{\boldsymbol{v}} \\ \delta\dot{\boldsymbol{\omega}}\end{bmatrix} = A\begin{bmatrix}\delta\boldsymbol{r} \\ \delta\dot{\boldsymbol{r}} \\ \delta\boldsymbol{q}_{\boldsymbol{v}} \\ \delta\boldsymbol{\omega}\end{bmatrix} \tag{31}$$

$$\begin{bmatrix}\delta\dot{\boldsymbol{r}} \\ \delta\ddot{\boldsymbol{r}} \\ \delta\dot{\boldsymbol{q}}_{\boldsymbol{v}} \\ \delta\dot{\boldsymbol{\omega}}\end{bmatrix} = \begin{bmatrix} 0 & \underline{1} & 0 & 0 \\ a_{21} & 0 & a_{23} & 0 \\ 0 & 0 & 0 & \frac{1}{2}q_{ve}^\times \\ a_{41} & 0 & a_{43} & 0 \end{bmatrix}\begin{bmatrix}\delta\boldsymbol{r} \\ \delta\dot{\boldsymbol{r}} \\ \delta\boldsymbol{q}_{\boldsymbol{v}} \\ \delta\boldsymbol{\omega}\end{bmatrix} \tag{32}$$

$$\delta\dot{\boldsymbol{r}} = \delta\dot{\boldsymbol{r}} \tag{33}$$

$$\delta\dot{\boldsymbol{q}}_{\boldsymbol{v}} = \frac{1}{2}q_{ve}\times\delta\omega \tag{34}$$

$$\delta\ddot{\boldsymbol{r}} = a_{21}\delta\boldsymbol{r} + a_{23}\delta\boldsymbol{q}_{\boldsymbol{v}} \tag{35}$$

$$\delta\dot{\boldsymbol{\omega}} = a_{41}\delta\boldsymbol{r} + a_{43}\delta\boldsymbol{q}_{\boldsymbol{v}} \tag{36}$$

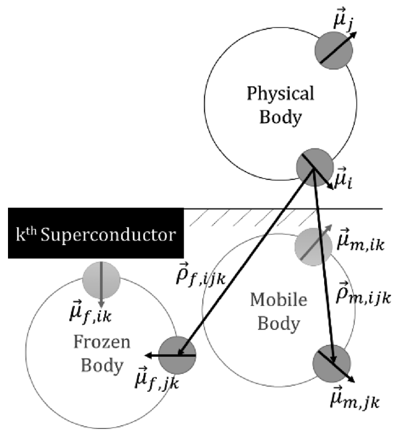

Fig. 4. Frozen and mobile images from magnet *j* acting on magnet *i* across superconductor *k*.

IV. Linearized Rigid Body Dynamics for an Arbitrary Number of Magnets and Superconductors

For a system of M rigidly constrained magnets on a rigid body with each magnet flux pinned to N fixed superconductors, each superconductor will store M frozen images. The system of permanent magnets will feel the effect of each Nth superconductor's embedded images, in which each superconductor holds M frozen images, totaling $M \times N$ frozen images. An equal number of mobile images pair with the frozen image counterparts, yielding a total $2 \times M \times N$ images that generate forces and torques. Assuming the magnets are rigidly mounted together, the summation of the forces on each magnet yields the total force on the body at the magnet bodies' center of mass.

A single flux-pinned interaction happens between the images of magnets i and j, in which magnet j produces frozen and mobile images on superconductor k, given by (41) and shown in Fig. 4. Magnet j produces frozen and mobile images on multiple superconductors, which all affect magnet i. The total contribution of magnet j's images onto magnet i is the summation of all individual flux-pinned interactions between magnets i and j across all superconductors, given by (42). The total force on magnet i from all magnet images is the sum of all magnet j influences across all superconductors, given by (43). The total force on a rigid body is the summation of total force on each magnet I, given by (44).

The torque is similar to the force summation with an extra term attributed to the force with a moment arm on magnet i, given by (45). The total torque on a rigid body is analogous to the total force equation but also includes a torque from each force displaced from the center of mass, given by (46). These two summation equations can be rearranged into a linear set of equations using the same linearization techniques from the single magnet single superconductor case.

$$\boldsymbol{F}_{ijk} = \boldsymbol{F}_{\mathbf{frozen}} + \boldsymbol{F}_{\mathbf{mobile}} \tag{41}$$

$$\boldsymbol{F}_{ij} = \sum_{k=1}^{M} (\boldsymbol{F}_{\mathbf{frozen}} + \boldsymbol{F}_{\mathbf{mobile}})_k \tag{42}$$

$$\boldsymbol{F}_{i} = \sum_{j=1}^{N} \sum_{k=1}^{M} ((\boldsymbol{F}_{\mathbf{frozen}} + \boldsymbol{F}_{\mathbf{mobile}})_k)_j \tag{43}$$

$$\boldsymbol{F}_{COM} = \sum_{i=1}^{N} \sum_{j=1}^{N} \sum_{k=1}^{M} \left(((\boldsymbol{F}_{\mathbf{frozen}} + \boldsymbol{F}_{\mathbf{mobile}})_k)_j\right)_i \tag{44}$$

$$\boldsymbol{\tau}_{i} = \sum_{j=1}^{N} \sum_{k=1}^{M} ((\boldsymbol{\tau}_{\mathbf{frozen}} + \boldsymbol{\tau}_{\mathbf{mobile}})_k)_j + \boldsymbol{\rho}_i \times \boldsymbol{F}_i \tag{45}$$

$$\boldsymbol{\tau}_{COM} = \sum_{i=1}^{N} \sum_{j=1}^{N} \sum_{k=1}^{M} \left(((\boldsymbol{\tau}_{\mathbf{frozen}} + \boldsymbol{\tau}_{\mathbf{mobile}})_k)_j\right)_i + \sum_{i=1}^{M} \boldsymbol{\rho}_i \times \boldsymbol{F}_i . \tag{46}$$

$$a_{21} = M^{-1} \frac{3\mu_0}{4\pi|\rho_e|^5} \begin{pmatrix} m_{fe}^{\times} m_e^{\times} + m_e^{\times} m_{fe}^{\times} - 2 m_e^T m_{fe} \underline{1} - \frac{5}{|\rho_e|^2} \left(\rho_e \left(\rho_e^{\times} m_{fe}\right)^T m_e^{\times} - \rho_e \left(\rho_e^{\times} m_e\right)^T m_{fe}^{\times} \right) + \\ -\frac{5}{|\rho_e|^2} \left(\left(\rho_e^{\times} m_e\right)^{\times} m_{fe} + \left(\rho_e^{\times} m_{fe}\right)^{\times} m_e - 2\left(m_e^T m_{fe}\right) \rho_e + \frac{5}{|\rho_e|^2} \left(\left(\rho_e^{\times} m_e\right)^T \left(\rho_e^{\times} m_{fe}\right)\right) \rho_e^T \right) + \\ 2\hat{m}_s \hat{m}_s^T \left(m_{me}^{\times} m_e^{\times} + m_e^{\times} m_{me}^{\times} - 2 m_e^T m_{me} \underline{1} - \frac{5}{|\rho_e|^2} \left(\rho_e \left(\rho_e^{\times} m_{me}\right)^T m_e^{\times} - \rho_e \left(\rho_e^{\times} m_e\right)^T m_{me}^{\times} \right) \right. \\ \left. -\frac{5}{|\rho_e|^2} \left(\left(\rho_e^{\times} m_e\right)^{\times} m_{me} + \left(\rho_e^{\times} m_{me}\right)^{\times} m_e - 2\left(m_e^T m_{me}\right) \rho_e + \frac{5}{|\rho_e|^2} \left(\left(\rho_e^{\times} m_e\right)^T \left(\rho_e^{\times} m_{me}\right)\right) \rho_e^T \right) \right) \end{pmatrix} \tag{37}$$

$$a_{23} = M^{-1} \frac{3\mu_0 |m_e|}{4\pi|\rho_e|^5} \begin{pmatrix} -m_{fe}^{\times} \rho_e^{\times} + \left(\rho_e^{\times} m_{fe}\right)^{\times} - 2\rho_e m_{fe}^T + \frac{5}{|\rho_e|^2} \rho_e \left(\rho_e^{\times} m_{fe}\right)^T \rho_e^{\times} + \\ -m_{me}^{\times} \rho_e^{\times} + \left(\rho_e^{\times} m_{me}\right)^{\times} - 2\rho_e m_{me}^T + \frac{5}{|\rho_e|^2} \rho_e \left(\rho_e^{\times} m_{me}\right)^T \rho_e^{\times} + \\ \left(\underline{1} - 2\hat{m}_s \hat{m}_s^T\right) \left((\rho_e m_e)^{\times} - m_e^{\times} \rho_e^{\times} - 2\rho_e m_e^T + \frac{5}{|\rho_e|^2} \rho_e \left(\rho_e^{\times} m_e\right)^T \rho_e^{\times} \right) \end{pmatrix} \tag{38}$$

$$a_{41} = I^{-1} \frac{\mu_0}{4\pi|\rho_e|^3} \begin{pmatrix} \frac{3}{|\rho_e|^2} \left(m_e^T \rho_e m_{fe}^{\times} + m_{fe}^T \rho_e m_e^{\times} - \left(\frac{3}{|\rho_e|^2} m_e^T \rho_e m_{fe}^{\times} \rho_e + m_e^{\times} m_{fe} \right) \rho_e^T \right) + \\ 2\hat{m}_s \hat{m}_s^T \left(\frac{3}{|\rho_e|^2} \left(m_e^T \rho_e m_{me}^{\times} + m_{me}^T \rho_e m_e^{\times} - \left(\frac{3}{|\rho_e|^2} m_e^T \rho_e m_{me}^{\times} \rho_e + m_e^{\times} m_{me} \right) \rho_e^T \right) \right) \end{pmatrix} \tag{39}$$

$$a_{43} = I^{-1} \frac{\mu_0 |m_e|}{4\pi|\rho_e|^3} \left(\frac{3}{|\rho_e|^2} m_{fe}^{\times} \rho_e \rho_e^T - m_{fe}^{\times} + \frac{3}{|\rho_e|^2} m_{me}^{\times} \rho_e \rho_e^T - m_{me}^{\times} + \left(2\hat{m}_s \hat{m}_s^T - \underline{1}\right) \left(\frac{3}{|\rho_e|^2} m_e^{\times} \rho_e \rho_e^T + m_e^{\times} \right) \right). \tag{40}$$

The state space of the single magnet single superconductor case has 12 state variables: translational position, translational velocity, quaternion vector, and angular velocity of the magnet. For the general case of an M magnet N superconductor interaction, the states will include those 12 state variables for each magnet on the rigid body, i.e., $12M$ total states. The most general plant, given in (47), is a simplification of the multiple magnet and multiple superconductor plant to a matrix of block matrices, where $\delta z_i = [\delta \boldsymbol{r}_i \delta \dot{\boldsymbol{r}}_i \delta \boldsymbol{q}_{vi} \delta \boldsymbol{\omega}_i]^T$ and $A_{\mathrm{i,j}}$ is the linearized dynamics of magnet i due to magnet j's images.

$$\begin{bmatrix} \delta \dot{z}_1 \\ \vdots \\ \delta \dot{z}_m \end{bmatrix} = \begin{bmatrix} A_{1,1} & \cdots & A_{1,M} \\ \vdots & \ddots & \vdots \\ A_{M,1} & \cdots & A_{M,M} \end{bmatrix} \begin{bmatrix} \delta z_1 \\ \vdots \\ \delta z_m \end{bmatrix} \tag{47}$$

Four Jacobians provide the basis for the partitions in the $A_{i,j}$ matrix of (47): force and torque as a function of position and orientation. The single magnet and single superconductor plant is derived using this general form $A_{i,j}$, given by (48). The magnet images affecting the dynamics can be from any magnet's images embedded in any superconductor. Every interaction is pairwise and all block matrices are populated. The larger system variables are analogous to the single magnet and single superconductor variables in (33)–(40). The velocity of magnet i is only the velocity of magnet j, when $i = j$. The quaternion derivative of magnet i is only propagated when magnet $j = i$. Any magnetic moment dipole from an image is established from magnet j about superconductor k. Any magnetic moment dipole from a magnet is established from magnet i. The distance vectors are calculated from magnet j's images about superconductor k to magnet i. These equations constitute the entries of the linearized state matrix, forming the basis of a linearized flux-pinning dynamics model for magnet i from specific magnet j's images from superconductor k. $a_{21,ij}$, $a_{23,ij}$, $a_{41,ij}$, and $a_{43,ij}$ are expressions with summation over all N superconductors.

$$\begin{bmatrix} \delta \dot{\boldsymbol{r}}_i \\ \delta \ddot{\boldsymbol{r}}_i \\ \delta \dot{\boldsymbol{q}}_{vi} \\ \delta \dot{\boldsymbol{\omega}}_i \end{bmatrix} = A_{i,j} \begin{bmatrix} \delta \boldsymbol{r}_j \\ \delta \dot{\boldsymbol{r}}_j \\ \delta \boldsymbol{q}_{vj} \\ \delta \boldsymbol{\omega}_j \end{bmatrix} \tag{48}$$

where

$$A_{i,j} = \begin{bmatrix} 0 & a_{12,ij} & 0 & 0 \\ a_{21,ij} & 0 & a_{23,ij} & 0 \\ 0 & 0 & 0 & a_{34,ij} \\ a_{41,ij} & 0 & a_{43,ij} & 0 \end{bmatrix}.$$

The output states of a rigid body about the center of mass are translational position, translational velocity, attitude, and angular velocity of the magnet. For the M magnet N superconductor case, the input state includes the position, velocity, attitude, and angular velocity of every magnet j, where A_j represents the contribution to body dynamics from magnet j's state, given by (49). $a_{21,j}$, $a_{23,j}$, $a_{41,j}$, and $a_{43,j}$ are expressions with summation over all N superconductors and M magnets. An analogous operation would be to sum each $A_{i,j}$ block matrix along each column or ith index, resulting in A_j. These 3×3 block matrices form the basis of a linearized flux-pinning dynamics model for a rigid body with all M magnets.

$$\begin{bmatrix} \delta \dot{\boldsymbol{r}}_{COM} \\ \delta \ddot{\boldsymbol{r}}_{COM} \\ \delta \dot{\boldsymbol{q}}_{vCOM} \\ \delta \dot{\boldsymbol{\omega}}_{COM} \end{bmatrix} = \begin{bmatrix} A_1 & \ldots & A_M \end{bmatrix} \begin{bmatrix} \delta \boldsymbol{r}_1 \\ \delta \dot{\boldsymbol{r}}_1 \\ \delta \boldsymbol{q}_{v1} \\ \delta \boldsymbol{\omega}_1 \\ \vdots \\ \delta \boldsymbol{r}_m \\ \delta \dot{\boldsymbol{r}}_m \\ \delta \boldsymbol{q}_{vM} \\ \delta \boldsymbol{\omega}_m \end{bmatrix} \tag{49}$$

where

$$A_{i,j} = \begin{bmatrix} 0 & a_{12,ij} & 0 & 0 \\ a_{21,ij} & 0 & a_{23,ij} & 0 \\ 0 & 0 & 0 & a_{34,ij} \\ a_{41,ij} & 0 & a_{43,ij} & 0 \end{bmatrix}.$$

V. Sensitivity and Comparison of Single Magnet and Single Superconductor Dynamics

To validate the linearized dynamics and investigate the dynamic sensitivity of each state, a simulation with the full nonlinear dynamic equations is compared to the linearized state space. The fully nonlinear simulation also offers a second method to validate the linearized state space, using a common software package. Dynamic characteristics of the linearized state space are discussed, followed by a comparison of the nonlinear dynamic time histories and the derived linearized state-space-propagated dynamics to generate the RMS error. Finally, this paper studies the sensitivity of force and torque by independently varying each state.

A. *Defining System Parameters*

The specific magnet chosen is that of strength 0.8815 T and diameter 0.75 in. If z represents the vertical height in the Cartesian coordinate space, the magnet is field-cooled 1 cm above the superconductor. Both the superconductor and magnet are pointing directly upward. The position of the permanent magnet from an arbitrary origin on the superconductor surface is represented by $\boldsymbol{r}_1$. The magnetic moment dipole of the permanent magnet contains a field strength and a unit direction, represented by $\boldsymbol{m}_1$. The orientation of the superconductor is the surface normal unit vector, given by $\hat{\boldsymbol{m}}_s$. The mass matrix is the mass of the permanent magnet, multiplied by an identity matrix, given by M. R is the radius of the spherical magnetic moment dipole. I is the inertia tensor of the spherical magnet.

From these physical parameters, the image parameters are found. $\boldsymbol{r}_f$ is the position of the frozen image. $\boldsymbol{r}_m$ is the position of the mobile image. $\boldsymbol{\rho}_e$ is the position vector from the images

TABLE I
SINGLE MAGNET AND SUPERCONDUCTOR CASE STUDY PARAMETERS

Distance [m]	Magnet Moment Dipole [T]	Body Parameters
$\boldsymbol{r_1}$ = [0; 0; 0.01]	$\boldsymbol{m_1}$ = 0.8815[0; 0; 1]	$\hat{m}_s$ = [0; 0; 1]
$\boldsymbol{\rho_e}$ = [0; 0; 0.02]	$\boldsymbol{m_e}$ = 0.8815[0; 0; 1]	M = 0.0272 kg
$\boldsymbol{r_f}$ = [0; 0; −0.01]	$\boldsymbol{m_{fe}}$ = 0.8815[0; 0; 1]	R = 0.009525m
$\boldsymbol{r_m}$ = [0; 0; −0.01]	$\boldsymbol{m_{me}}$ = 0.8815[0; 0; −1]	$I = 3.63 \times 10^{-5}$ kg-m^2

to the permanent magnet when in equilibrium, which is also the field-cooled position. The equilibrium magnetic moment dipole is equivalent to the field-cooled orientation of the permanent magnet $\boldsymbol{m_e}$. The frozen-image magnetic moment dipole $\boldsymbol{m_{fe}}$ is of the same orientation as the permanent magnet orientation when field-cooled. The mobile image magnetic moment dipole $\boldsymbol{m_{me}}$ is the mirrored orientation as the permanent magnet orientation when field-cooled. Table I presents a complete list of system parameters. All code is online and available at github.com/frankiezoo/SMSS Linear Dynamics.git.

B. Linearizing a Nonlinear Simulation and Deriving Linearized Matrix

After building a nonlinear dynamics model of a single magnet and single superconductor, the model is linearized with the help of the Linear Analysis Toolbox from MathWorks Simulink. The input perturbation states are the quaternion and the position of the permanent magnet. The output measurement is the force and torque. The state space produced from Simulink's linearization produces (50). The single magnet and single superconductor plant from (32) is modified to include the four Jacobians from Simulink's linearization process from (49), given by (51). The state matrix generated from the simulation is equivalent within machine precision to the linearized state matrix derived in the preceding sections.

$$J = \begin{bmatrix} \frac{\partial \boldsymbol{F}}{\partial \boldsymbol{r}} & \frac{\partial \boldsymbol{F}}{\partial \boldsymbol{q}} \\ \frac{\partial \boldsymbol{\tau}}{\partial \boldsymbol{r}} & \frac{\partial \boldsymbol{\tau}}{\partial \boldsymbol{q}} \end{bmatrix} \tag{50}$$

$$\begin{bmatrix} \delta\dot{\boldsymbol{r}} \\ \delta\ddot{\boldsymbol{r}} \\ \delta\dot{\boldsymbol{q}}_v \\ \delta\dot{\boldsymbol{\omega}} \end{bmatrix} = \begin{bmatrix} 0 & \underline{1} & 0 & 0 \\ M^{-1}\frac{\partial \boldsymbol{F}}{\partial \boldsymbol{r}} & 0 & M^{-1}\left|\boldsymbol{m}_e\right|\frac{\partial \boldsymbol{F}}{\partial \boldsymbol{q}} & 0 \\ 0 & 0 & 0 & \frac{1}{2}q_{ve}^{\times} \\ I^{-1}\frac{\partial \boldsymbol{\tau}}{\partial \boldsymbol{r}} & 0 & I^{-1}\left|\boldsymbol{m}_e\right|\frac{\partial \boldsymbol{\tau}}{\partial \boldsymbol{q}} & 0 \end{bmatrix} \begin{bmatrix} \delta\boldsymbol{r} \\ \delta\dot{\boldsymbol{r}} \\ \delta\boldsymbol{q}_v \\ \delta\boldsymbol{\omega} \end{bmatrix}. \tag{51}$$

C. Modal Analysis of Linearized Flux-Pinned Model

Modal analysis of a dynamic system reveals stability and frequency information. The eigenvalues and eigenvectors are found with the linearized state-space matrix. The plant derived in Section V-B has the following eigenpairs. The flux-pinned system is marginally stable because all eigenvalues have a 0 real component. The numerical values associated with each eigenpair manifest different properties in the physical system, as shown in Table II.

TABLE II
SINGLE MAGNET AND SUPERCONDUCTOR EIGENPAIRS

eigenpair	λ	mode	shape
1	108.5i	ω_y	$\dot{r}_x$
2	-108.5i	ω_y	$\dot{r}_x$
3	108.5i	ω_x	$\dot{r}_y$
4	-108.5i	ω_x	$\dot{r}_y$
5	37.4i	ω_x	ω_y
6	-37.4i	ω_x	ω_y
7	37.4i	ω_y	ω_x
8	-37.4i	ω_y	ω_x
9	146.4i	$\dot{r}_z$	r_z
10	-146.4i	$\dot{r}_z$	r_z
11	0	q_3	r_z
12	0	q_3	

The first ten eigenvalues of the flux-pinned plant are all imaginary, which represent the spring-like nature of flux-pinned interfaces. Due to the axial symmetry of the magnet, the eigenvalues representing the x and y dynamics come in quadruplets. The eigenvectors with imaginary values must be paired with the conjugate eigenvector to manifest real physical dynamics. Intuitively, flux-pinned interfaces have stiffer translational joints than rotational joints. The modal analysis reveals the same conclusion, where the z translation has the highest stiffness, the x and y translations are also relatively high, and the x and y rotations have the lowest stiffness.

The first four modes show a relation between the rotation and translation about the x and y axes. The rotation is the main modal shape, but contributes to the translation. This stiffness is rather high. The next four modes, 5–8, show a relation between the rotation about the x and y axes. The rotation about one axis is the main modal shape, but the rotation about the other axis is also a significant modal. This stiffness is the lowest of all modes. Modes 9 and 10 strictly reflect translation in the z direction. It has the highest stiffness of all the modes. The last modes have 0 eigenvalues because the dynamics of the system do not resist to any perturbation of these states. Any perturbation in q_3, or the magnetic strength of the magnet, results in translation in the z direction. Any perturbation in the rotation about the z-axis q_3 results in rotation about the z-axis until another perturbation or energy dissipation is introduced.

D. Sensitivity of Linearized Dynamics due to State Variation

Although the linearized plant is nearly exact to machine precision error at equilibrium, the linear plant approximates nonlinear dynamics less accurately the further the system deviates from equilibrium. Figs. 5–9 show sensitivity plots varying state variables and correlating error in force and torque calculations between the linearized equations and nonlinear equations. The translation and rotation in the x and y directions are the same due

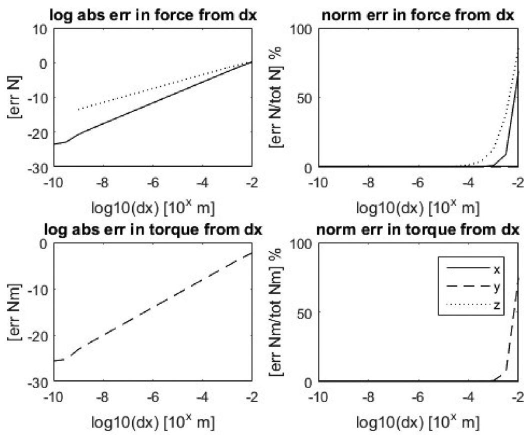

Fig. 5. Error in force and torque between linearized and nonlinear models when varying displacement along the *x* direction.

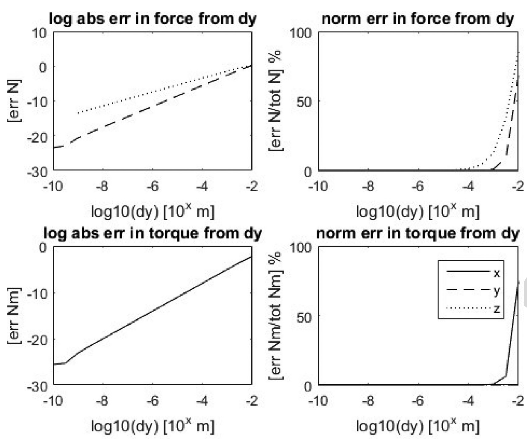

Fig. 6. Error in force and torque between linearized and nonlinear models when varying displacement along the *y* direction.

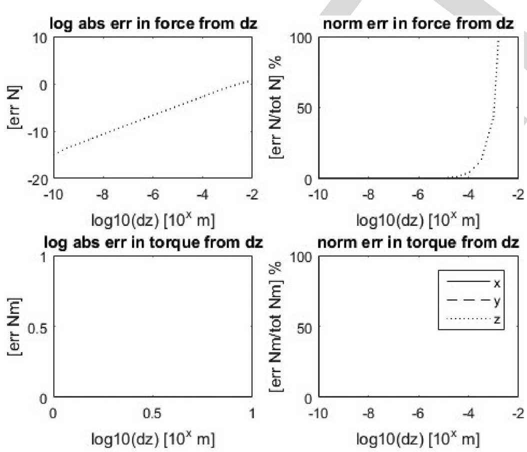

Fig. 7. Error in force and torque between linearized and nonlinear models when varying displacement along the *z* direction.

to symmetry, as shown in Figs. 5, 6, 8, and 9. There is no rotation in the *z* direction because the magnet is axially symmetric. The most sensitive state is the translational displacement in the *z* direction, as shown in Fig. 7. The equilibrium separation distance from the superconductor surface is 1 cm, or 10^{-2} m. To retain

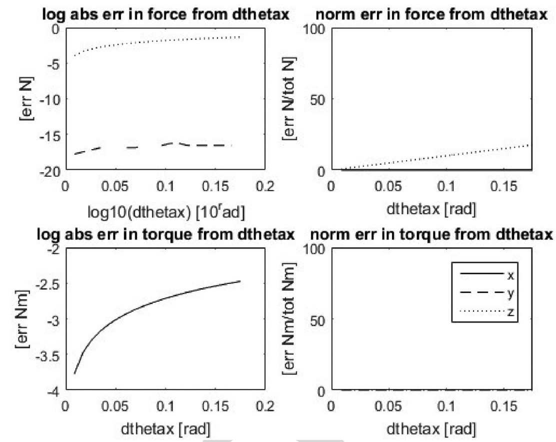

Fig. 8. Error in force and torque between linearized and nonlinear models when varying rotation along the *x* direction.

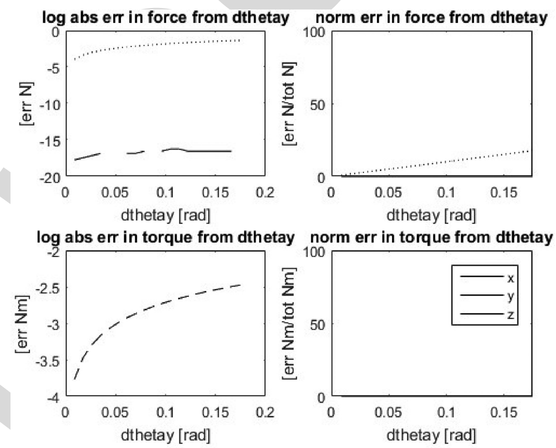

Fig. 9. Error in force and torque between linearized and nonlinear models when varying rotation along the *y* direction.

below 5% error in force, displacements in the *z* direction must be bound to 10^{-4} m. This requirement is much more stringent if the error threshold is 1%, decreasing the displacement bound down to 10^{-5} m. Perturbations in the *x* and *y* translational displacements may be as high as 1 m, or 10^{-3} m, yet still retaining 5% RMS error in force.

VI. Conclusion

The general, linearized state-space equations derived here allow the closed-form analytical characterization of a flux-pinned interface, along with the state matrix needed to formulate linear control algorithms. The results are an important step toward implementing six degree-of-freedom dynamic systems, such as docking, formation flying, autonomous assembly of multiple bodies, and noncontacting pointing platforms.

This model is expected to help characterize the passive dynamics of a flux-pinned system in all its degrees of freedom to permit the formulation of control algorithms. The linearized model accurately reflects the nonlinear dynamics within small displacements. Understanding the sensitivity of spatial perturbations informs the implementation of feedback control, for example, in choosing the proper sensor resolution and predicting the expected excursions of the flux-pinned interface dynamics.

Although the linearized equations are consistent with the fundamental physics, Kordyuk's geometric mapping and Villani's dipole interactions represent limitations that may come into play for systems with nonlinear excursions and for which the dipole assumptions break down. Future work lies in refining the basic nonlinear flux-pinning model and parameterizing the nonlinearities in the dynamics model.

References

[1] S. Earnshaw, "On the nature of the molecular forces which regulate the constitution of the luminiferous ether," *Trans. Camb. Philos. Soc.*, vol. 7, pp. 97–112, 1842.

[2] R. Williams and J. R. Matey, "Equilibrium of a magnet floating above a superconducting disk," *Appl. Phys. Lett.*, vol. 52, no. 9, pp. 751–753, Feb. 1988.

[3] C. Navau, N. Del-Valle, and A. Sanchez, "Macroscopic modeling of magnetization and levitation of hard type-II superconductors: The critical-state model," *IEEE Trans. Appl. Supercond.*, vol. 23, no. 1, Feb. 2013, Art. no. 8201023.

[4] A. A. Kordyuk, "Magnetic levitation for hard superconductors," *J. Appl. Phys.*, vol. 83, no. 1, pp. 610–612, Jan. 1998.

[5] F. Zhu, L. Jones-Wilson, and M. Peck, "Flux-pinned dynamics model parameterization and sensitivity study," presented at the IEEE Aerospace Conf., Big Sky, Montana, 2018.

[6] Y. Yang and X. Zheng, "Method for solution of the interaction between superconductor and permanent magnet," *J. Appl. Phys.*, vol. 101, no. 11, Jun. 2007, Art. no. 113922.

[7] K. W. Yung, P. B. Landecker, and D. D. Villani, "An analytic solution for the force between two magnetic dipoles," *Phys. Sep. Sci. Eng.*, vol. 101, no. 11, pp. 39–52, 1998.

[8] P. B. Landecker, D. D. Villani, and K. W. Yung, "An analytic solution for the torque between two magnetic dipoles," *Phys. Sep. Sci. Eng.*, vol. 10, no. 1, pp. 29–33, 1999.

[9] M. K. Alqadi, F. Y. Alzoubi, H. M. Al-khateeb, and N. Y. Ayoub, "Interaction between a point magnetic dipole and a high-temperature superconducting sphere," *Phys. B: Condens. Matter*, vol. 404, no. 12, pp. 1781–1784, Jun. 2009.

[10] A. Cansiz, J. R. Hull, and Ö. Gundogdu, "Translational and rotational dynamic analysis of a superconducting levitation system," *Supercond. Sci. Technol.*, vol. 18, no. 7, 2005, Art. no. 990.

[11] T. Sugiura, H. Ura, and K. Kuroda, "Magnetic stiffness of a coupled high-T_c superconducting levitation system," *Phys. C: Supercond.*, vol. 392, pp. 648–653, 2003.

[12] L. Jones and M. Peck, "Control strategies utilizing the physics of flux-pinned interfaces for spacecraft," in *Proc. AIAA Guidance, Navigation, Control Conf.*

[13] T. Chow, *Introduction to Electromagnetic Theory: A Modern Perspective*. Boston, MA, USA: Jones & Bartlett, 2006.

Frances Zhu received the B.S. degree in mechanical and aerospace engineering from Cornell University, Ithaca, NY, USA, in 2014, where she is currently working toward the Ph.D. degree in aerospace engineering.

Since 2014, she has been a Research Assistant with the Space Systems Design Studio, Ithaca, NY, USA, specializing in dynamics, systems, and controls engineering. Her research interests include flux-pinned interface applications, spacecraft system architectures, robot dynamics, estimation, and controls.

Ms. Zhu is a NASA Space Technology Research Fellow.

Mason A. Peck received the B.S. degree in aerospace engineering from the University of Texas at Austin, Austin, TX, USA, and the M.S. and Ph.D. degrees from the University of California, Los Angeles, Los Angeles, CA, USA, as a Howard Hughes Fellow from 1998 to 2001.

From 1993 to 1994, he worked at Bell Helicopter on structural dynamics. From 1994 to 2001, he was an Attitude Dynamics Specialist and Systems Engineer at Hughes Space and Communications (now Boeing Satellite Systems). During his years at Boeing, he served as Attitude Dynamics Lead in the Boeing Mission Control Center, participating in real-time spacecraft operations and helping to resolve spacecraft performance anomalies. In 2001, he joined Honeywell Defense and Space Systems, and in 2003 was named Principal Fellow. He has several patents on his name. In July 2004, he joined as a Faculty at Cornell University, where he teaches courses in dynamics and control and in the mechanical and aerospace engineering program, where he was promoted to an Associate Professor in fall 2010. In 2012, he was appointed as NASA's Chief Technologist.

GENERAL INSTRUCTION

- Authors: Please note that we cannot accept new source files as corrections for your paper. If possible, please annotate the PDF proof we have sent you with your corrections and upload it via the Author Gateway. Alternatively, you may send us your corrections in list format. You may also upload revised graphics via the Author Gateway.

QUERIES

Q1. Author: Fig. 1 is not cited in the text. Please cite it at an appropriate place.

Q2. Author: The word axis and direction has been added after x, y and z here and elsewhere in the text and figure captions. Please check for correctness.

Q3. Author: Please provide the page range for reference [12].

Q4. Author: Please mention the years in which Mason. A Peck received the B.S., M.S., and Ph.D. degrees.